WELL TEST INTERPRETATION USING LAPLACE SPACE TYPE CURVES

By
Marcel Bourgeois
Elf Aquitaine

April 1992

Contents

Acknowledgements

This work, which summarizes 18 months of research at Stanford University, is part of the Stanford Well Testing Industrial Affiliates Program (SUPRI-D). It was conducted under the direction of Professor Roland N. Horne, and I am deeply appreciative of his advice, guidance and encouragement throughout our friendly but fruitful collaboration.

I would also like to express my gratitude to ELF Aquitaine that provided me with adequate preparation and material support for this research.

Abstract

This study presents the mathematical background which justifies the use of Laplace space in well test analysis. It enables us to perform the whole parameter identification (C_D, $Skin$, kh, ...) in Laplace space, or at least gives us a powerful tool to treat the pressure data in order to recognize the model to use for the parameter identification in real space. It shows a manner in which the Laplace transform can be plotted, showing exactly the same behaviour as the real pressure function so the plots keep their familiar shape. The coefficients of the dimensionless parameters remain the same, too. This enables us to display a new set of characteristic and easily understandable type curves in Laplace space.

The mathematical background also sheds light on the use of the Laplace transform to achieve flowrate deconvolution, using modifications of earlier techniques which had been found to be extremely sensitive to noise in the data.

The treatments displayed are numerically stable, and it is explained why numerical instability can occur in flowrate deconvolution. The effectiveness of the treatments is explained whenever possible, and the effect of the late-time extrapolation is discussed as well.

The Laplace space approach provides an entirely new way of examining and understanding well test results. It has been succesfully applied to noisy, simulated data where a conventionnal interpretation could not illuminate ambiguities.

Chapter 1

Introduction

There are many techniques available for solving the problem of transient flow of slightly compressible fluids in porous media. One of them is the use of the Laplace transform, which has many convenient properties (van Everdingen and Hurst, Ref. [1]). Since the diffusivity equation is usually simpler in Laplace space than in real space, solutions may be determined for most well configurations, which correspond to different boundary conditions. Previous investigations, particularly Ozkan and Raghavan (Ref. [2, 3]), provide extensive libraries of computable solutions to a great variety of well test problems. The analytical solutions are therefore usually better known in Laplace space than in real space. In addition to this, evaluating the solution in Laplace space makes it very easy to take into account the double porosity behaviour of a fissured reservoir.

Despite all these advantages, the Laplace transform often remains abstruse and somewhat "user-unfriendly", because methods of direct interpretation rely on the visualization of the solution in real space, in order to recognize the reservoir model.

This study investigates a way of presenting the Laplace transform of the transient wellbore pressure which makes it directly interpretable. It allows us to create characteristic type curves, and therefore to perform model recognition in Laplace space. Eventually, the whole parameter identification can be performed in Laplace space, which reduces the need for numerical inverters. This, as discussed in the last chapter, is interesting when the data are not

monotonic and the time consuming algorithm developed by Crump [4] has to be used instead of Stehfest's algorithm [5]. Working more in Laplace space can therefore save a lot of mathematical treatment, which is all the more profitable when numerous iterations are to be performed, such as in non-linear regression, also known as automated type-curve matching (Rosa and Horne, Ref. [6]), one of the more promising modern well test identification methods.

The new understanding of the properties of the Laplace space solutions has enabled the development of a new method for deconvolving flowrate variations with noisy data. Basically, flowrate deconvolution has a very simple expression in Laplace space for perfect data, but numerical instability, which is inherent to the process, can cause problems. Constrained methods (Kuchuk et al., [7]) can be used to perform deconvolution despite this instability, but this study shows a simpler and quicker treatment, even in cases when no flowrate measurements are available.

This work therefore expands our ability to solve problems of transient flow with a simple yet powerful approach.

This work has been presented at the Society of Petroleum Engineers Fall Meeting in Dallas (Oct.7th, 1991) as paper # 22682, and the last results have been presented at the student paper contest during the Western Regional Meeting in Bakersfield (March 30th, 1992). It has been accepted for publication in SPE Formation and Evaluation.

Chapter 2

Mathematical Background

2.1 Considerations of Dimension

With fully dimensional variables, s_f is defined as the Laplace variable (as opposed to the dimensionless Laplace variable traditionally noted s), after which the definition of the Laplace transform is:

$$L\{p(t)\} \ = \overline{p}(s_f) \ = \int_{t=0}^{\infty} e^{-s_f \ t} \ p(t) \ dt \tag{2.1}$$

The dimension of $\overline{p}(s_f)$ is therefore time $\cdot$ pressure, which is not very convenient. It is much more interesting to work with the new expression, which we will call Laplace pressure:

$$s_f \ L\{p(t)\} \ = \ s_f \ \overline{p}(s_f) \tag{2.2}$$

This expression has the dimension of a pressure, and will therefore be expressed in psi if oilfield units are chosen, or in bar or Pascal . It should be emphasized that the operator, which acting on the real pressure $p(t)$ results in the Laplace pressure $s_f \cdot \overline{p}(s_f)$, has a very useful linear behavior, which will enable us to perform unit conversions or multiplications: For example, if $p_0 = 1$, we have $s_f \overline{p_0}(s_f) = 1$, and thus:

$$s_f \ (\overline{a \ + \ b \cdot p}) \ = \ a \ + \ b \cdot s_f \overline{p} \tag{2.3}$$

In these equations, s_f has the dimension of a reciprocal time, and the reader should always keep in mind that large values of s_f correspond to small values of t, because the contribution of the pressure to the Laplace integral is significant only at early times if s_f is large. Conversely, if the values of s_f are small, the contribution to the Laplace integral will cover the whole time range, until late time.

It is a common approach to work with dimensionless quantities, in order to keep familiar values even if the scale or the properties of well and reservoir are changed, or if the unit system changes. The definitions are, in consistent units:

$$p_D = \frac{2\pi\ k\ h}{qB\ \mu}\ \Delta p = \frac{\Delta p}{\alpha_p} \tag{2.4}$$

$$t_D = \frac{k\ t}{\phi\ \mu\ c_t\ r_w^2} = \frac{t}{\alpha_t} \tag{2.5}$$

$$C_D = \frac{C}{2\pi\ h\ \phi\ c_t\ r_w^2} = \frac{C}{\alpha_C} \tag{2.6}$$

In oilfield units, the definitions are:

$$p_D = \frac{k\ h}{141.2\ qB\ \mu}\ \Delta p \tag{2.7}$$

$$t_D = \frac{0.000264\ k\ t}{\phi\ \mu\ c_t\ r_w^2} \tag{2.8}$$

$$C_D = \frac{0.8936\ C}{h\ \phi\ c_t\ r_w^2} \tag{2.9}$$

The relation $\alpha_p = \alpha_t/\alpha_C$ is only true in consistent units. For the oilfield unit system, the equivalent relation is $\alpha_p = qB/24\ \cdot \alpha_t/\alpha_c$, because C is expressed in bbl/psi and not in hr/psi.

The definition of the dimensionless Laplace variable is:

$$s = s_f\ t/t_d = \alpha_t\ s_f \tag{2.10}$$

The dimensionless Laplace pressure is therefore:

$$s\ \overline{p_D}(s)\ =\ s\ \int_{t_D=0}^{\infty}\ e^{-st_D}\ p_D(t_D)\ dt_D\ =\ \frac{2\pi\ k\ h}{qB\ \mu}\ s_f\ \overline{\Delta p}(s_f) \tag{2.11}$$

The proportionality coefficient α_p between dimensionless and full dimension Laplace pressure remains the same as in real space, which is very convenient:

$$s\ \overline{p_D}(s)\ =\ s_f\ \overline{\Delta p}(s_f)\ /\alpha_p \tag{2.12}$$

For the skin S, the dimensional pressure drop across the skin is related to the dimensionless skin factor the following way:

$$\Delta p_S\ =\ \alpha_p\ S \tag{2.13}$$

2.2 Flowrate Deconvolution

The convolution of two functions in real space is equivalent to the product of their Laplace transforms in Laplace space. The pressure drop in the wellbore (assuming no skin) is the convolution integral of the Kernel function K with the derivative of the sandface flowrate:

$$p_D(t_D)\ =\ \int_{\tau=0}^{t_D}\ K(t_D-\tau)\ \frac{\partial q_{sf_D}(\tau)}{\partial\tau}\ d\tau \tag{2.14}$$

Thus in Laplace space:

$$\overline{p_D}(s)\ =\ \overline{K}(s)\ \cdot\ s\ \overline{q_{sf_D}}(s) \tag{2.15}$$

Here p_D is the pressure drop which actually occured due to the (variable) sandface flowrate q_{sf_D} ($=q_{sf}/q_{reference}$), and K is the pressure drop which would have occured had the well been opened to flow at constant rate ($q_{reference}$) at time zero. To yield the pressure drop in the well which would have occured if the flowrate had been a Heaviside step function (= Kernel function), the actual Laplace pressure drop is divided by the Laplace flowrate [1, 8]:

$$s\ \overline{K}(s)\ =\ \frac{s\ \overline{p_D}(s)}{s\ \overline{q_{sf_D}}(s)} \tag{2.16}$$

To compute the pressure drop in the wellbore for a constant wellbore storage C_D and skin S, the following formula can be used, which simply adds a skin pressure drop proportional to the actual sandface flowrate:

$$p_{wD}(t_D) \;=\; \int_{\tau=0}^{t_D} K(t_D-\tau)\;\frac{\partial q_{sf_D}(\tau)}{\partial \tau}\;d\tau \;+\; q_{sf_D}(t_D)\;S \tag{2.17}$$

In Laplace space:

$$s\;\overline{p_{wD}}(s) \;=\; s\;\overline{K}(s)\;\cdot\;s\;\overline{q_D}(s) \;+\; s\;\overline{q_D}(s)\;S \tag{2.18}$$

Knowing that the sandface flowrate is equal to the wellhead flowrate minus the wellbore unloading, we can say:

$$q_{sf_D} \;=\; q_{wh_D} \;-\; C_D\;\frac{\partial p_{wD}}{\partial t_D} \tag{2.19}$$

For a unit step wellhead flowrate, in Laplace space:

$$s\;\overline{q_{sf_D}} \;=\; 1 \;-\; C_D\;s^2\;\overline{p_{wD}}(s) \tag{2.20}$$

Rearranging this, p_{wD} can be expressed as a function of K, C_D and S:

$$s\;\overline{p_{wD}}(s) \;=\; \frac{s\overline{K}(s) \;+\; S}{1 \;+ C_D\;s\;(\;s\overline{K}(s) \;+\; S\;)} \tag{2.21}$$

Conversely, to remove C_D and S from a measured wellbore pressure:

$$s\;\overline{K}(s) \;=\; \frac{s\overline{p_{wD}}(s)}{1 \;- C_D\;s^2\;\overline{p_{wD}}(s)} \;-\; S \tag{2.22}$$

This relation is exact, but can be numerically unstable (due to division by zero) for wellbore storage deconvolution, if the data are noisy or if C_D is overestimated. This important practical problem is addressed later (see Eq. 3.58).

2.3 Initial And Final Value Theorem

Let us start with the initial value theorem, which is more intuitive. This theorem is true for any function that admits a Laplace transform. It is thus applicable to the flowrate and, what is of most interest for us, to the pressure, dimensionless or not. If the indicated limit exists, then:

$$\lim_{t \to 0} f(t) = \lim_{s_f \to \infty} s_f \overline{f}(s_f) \tag{2.23}$$

In particular :

$$\lim_{t \to 0} p(t) = \lim_{s_f \to \infty} s_f \overline{p}(s_f) \tag{2.24}$$

$$\lim_{t_D \to 0} p_D(t_D) = \lim_{s \to \infty} s \overline{p_D}(s) \tag{2.25}$$

For a drawdown test with wellbore storage, the linear early time behavior $p_D = t_D/C_D$ corresponds in Laplace space to $s\ \overline{p_D}(s) = 1/(sC_D)$, which is linear with respect to $(1/s)$. For a buildup test, both p_D and $s\ \overline{p_D}(s)$ tend to the shut-in pressure when $t_D \to 0$ and $s \to \infty$.

The final value theorem has a similar expression, but the limit is usually not finite for well test applications.

$$\lim_{t \to \infty} p(t) = \lim_{s_f \to 0} s_f \overline{p}(s_f) \tag{2.26}$$

$$\lim_{t_D \to \infty} p_D(t_D) = \lim_{s \to 0} s \overline{p_D}(s) \tag{2.27}$$

The exception where the limit is finite is a buildup test, where both expressions tend towards the initial pressure of the reservoir.

In both cases, the Laplace pressure and real pressure have a very similar behavior, demonstrating that the real space and Laplace space pressures range between the same values. This makes the Laplace pressure useful for visualization, as shown in section 3.2.

2.4 Semilog Behavior

We have seen that a linear behavior in real time corresponds to a linear behavior in Laplace space. This is transposable to a semilog behavior as well, although it is necessary to take account of the Euler constant $\gamma = 0.577215665...$:

$$\text{If} \quad f(t_D) = ln(t_D), \tag{2.28}$$

$$\text{then} \quad s\,\overline{f}(s) = -\gamma + ln(1/s) = ln(e^{-\gamma}/s) \tag{2.29}$$

$$\text{Thus if} \quad p_D(t_D) = a + b\,lnt_D\ , \tag{2.30}$$

$$\text{then} \quad s\,\overline{p_D}(s) = a - b\gamma + b\,ln(1/s) \tag{2.31}$$

Let us take the example of a vertical well, fully completed, in a homogeneous, infinite-acting reservoir. The solution to the diffusivity equation is well known, and can be expressed by means of the modified Bessel function of second kind and order zero and one. This cylindrical source solution can be approximated for the usual t_D range by the line source solution, for which we know the exact expression in real space, namely the exponential integral. In dimensionless terms, the solutions are:

$$\text{Cylindrical source:} \quad s\,\overline{K}(s) = \frac{K_0(r_D\sqrt{s})}{\sqrt{s}\ K_1(\sqrt{s})} \tag{2.32}$$

$$\text{Line source solution:} \quad s\,\overline{K}(s) = K_0(r_d\sqrt{s}) \tag{2.33}$$

$$\text{equivalent in real space to:} \quad K(t_D) = \frac{1}{2}\,E_1(\frac{r_D^2}{4\ t_D}) \tag{2.34}$$

The asymptotes at late time are respectively:

$$K(t_D) = \frac{1}{2}\,(\ ln(t_D) + \overbrace{2\ ln2\ -\ \gamma}^{0.809}\ ) \tag{2.35}$$

$$s\,\overline{K}(s) = \frac{1}{2}\,(\ ln(\frac{1}{s}) + 2\ ln2\ -\ 2\ \gamma) \tag{2.36}$$

Therefore, the plots $K(t_D)$ vs. t_D and $s\,\overline{K_D}(s)$ vs. $\frac{e^{-\gamma}}{s}$ have the same asymptote, which is the well-known semilog straight line. The plots in real

space and Laplace are not exactly the same, which is understable, but are mutually corresponding: to a real fuction corresponds a unique Laplace transform, and to a Laplace transform corresponds a unique original function. Nonetholess, the semilog regions of the plots of $K(t_D)$ vs. t_D and $s\ \overline{K}(s)$ vs. $\frac{1}{s}$ will have the same semilog slope, which will be $\ln(10)/2 \approx 1.15$ per log cycle, if the decimal logarithm is chosen. This interesting property, as well as the expression of the Laplace transform as computed in Romboutsos' algorithm (Ref. [11]), had already been found by Chaumet, Pouille and Séguier in 1962 (Ref. [9]).

Figure 2.1, shows a plot of the Kernel function for an infinite acting well and for the case of a linear boundary condition (constant pressure and no flow). Since both the diffusivity equation and the Laplace transform are linear with respect to the pressure (assuming Darcy flow), the superposition theorem holds and can be used to take the boundaries into account.
For example, for a reservoir with a sealing fault, the pressure drop in case of a stepwise flowrate can be computed using following expressions :

$$\text{Line source:}\quad s\ \overline{K}(s) \;=\; K_0(\sqrt{s}) \;+\; K_0(2r_{fD}\sqrt{s}) \tag{2.37}$$

$$\text{Cyl. source:}\quad s\ \overline{K}(s) \;=\; \frac{K_0(\sqrt{s}) \;+\; K_0(2r_{fD}\sqrt{s})}{\sqrt{s}\ K_1(\sqrt{s})} \tag{2.38}$$

If early time accuracy is needed, the cylindrical source expression should be used, since it is more exact and is not difficult to compute in Laplace space.

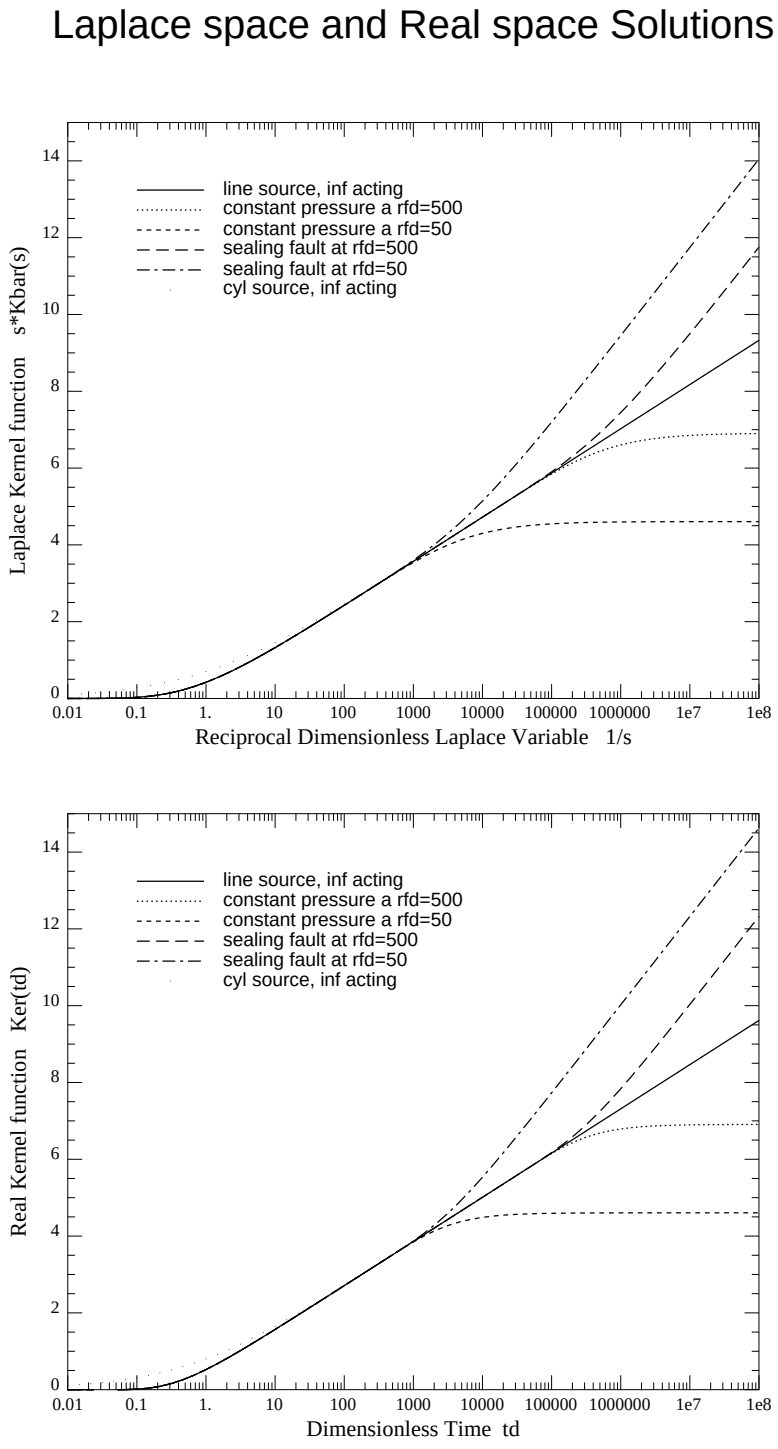

Figure 2.1: Dimensionless Kernel functions with different boundary conditions

Chapter 3

Applications

3.1 Forward Laplace Transform

To work in Laplace space, we need an algorithm to take the Laplace transform of real data. The algorithm described here is applicable to both flowrate or pressure data, but has been designed especially for the latter. The point is that this algorithm should be as accurate as possible, to avoid adding any systematic noise to the measurements, since that would be equivalent to losing information. As a matter of fact, the Laplace pressure can be seen to be an integration of the derivative of the real pressure, although it is not necessary to compute this derivative:

$$s_f \, \overline{p}(s_f) \;=\; s_f \int_{t=0}^{\infty} e^{-s_f t} \, p(t) \, dt \;=\; p(0^+) \;+\; \int_{t=0}^{\infty} e^{-s_f t} \, \frac{\partial p}{\partial t} \, dt \qquad (3.1)$$

Nevertheless, the Laplace pressure has a smoother behavior than the real pressure, but that is not always a disadvantage, since the derivative (with respect to $\ln(s)$ for example) of this expression is very diagnostic and remains smooth even for noisy original data, as will be shown in the examples.

One of the main problems is related to the fact that the Laplace transform, by definition, requires the knowledge of $p(t)$ over the whole time range, and that even a properly designed well test can give this information only partially. The pressure is measured only for a given time range (usually from about a second or a couple of seconds to a couple of days), and therefore

a meaningful Laplace pressure will only be available for a corresponding s range. For the time before and after the measurements, it will be necessary to extrapolate the data.

For early time, if wellbore storage is present, the pressure can be approximated linearly , although the small variations from a linear early time behavior represent the valuable information that can allow flowrate deconvolution. It is always good to have early time measurements, but it is not really necessary for taking the Laplace transform.

Between the measured data, the pressure was interpolated linearly, although spline fittings can be used as well. These methods already exist in the literature, so we will not expand upon this issue (Guillot and Horne, Ref. [10]).

The late time problem has to be addressed more carefully, however, since an exact Laplace transform of an interpolation of semilog behavior has often been reported to be problematic, because the analytic expression is difficult to derive properly.

It seems reasonable to make an extrapolation which will follow as close as possible the probable behavior of the data. Commonly, a semilog extrapolation will be chosen, but in case of a buildup, we can choose a semilog extrapolation with respect to Horner time. In case of a closed outer boundary, we can use a linear extrapolation, as described in Romboutsos and Stewart (Ref. [11]) algorithm. But even with a good extrapolation, there is a range for which the calculated Laplace transform is nothing more than a self-fulfilling prophecy, namely the transform of the extrapolation, while the pressure could actually have looked differently if the test had lasted longer. The limit until which the Laplace transform remains meaningful can be estimated as:

$$s_f \; > \; \frac{1}{t_{max}} \tag{3.2}$$

The actual contribution to the Laplace transform for $0 \; < t \; < \; t_{max}$, if t_{max} is the last data point, can be computed with the Romboutsos and Stewart (Ref. [11]) algorithm. The only difficult point is the contribution for $t \; > \; t_{max}$, which is a truncated integral of a logarithm, and not a translated integral; this confusion was at the origin of earlier miscalculations. The proper integration is:

$$I(s_f) \quad = \quad \int_{t=t_{max}}^{\infty} \; e^{-s_f t} \; ln(t/t_{max}) \; dt \tag{3.3}$$

$$= \frac{1}{s_f} \int_{t_{max}}^{\infty} \frac{e^{-s_f t}}{t}\, dt \quad \text{integrating by parts} \tag{3.4}$$

$$= \frac{1}{s_f}\, E_1(s_f\ t_{max}) \quad \text{exponential integral} \tag{3.5}$$

$$\neq e^{-s_f t_{max}}\ (\frac{-\gamma\ -\ ln(s_f)}{s_f}) \tag{3.6}$$

The complete algorithm we developed and successfully used in this work is therefore, if the notations are $f(t_i) = f_i$ for $i = 0$ to n, with $t_0 = 0$ (usually $f_0 = 0$) and $t_{max} = t_n$:

$$\overline{f}(s_f) \ = \ \frac{f_0}{s_f} \ + \ \sum_{i=0}^{n-1} \ \frac{f_{i+1} - f_i}{t_{i+1} - t_i} \cdot \frac{e^{-s_f t_i} - e^{-s_f t_{i+1}}}{s_f^2} \ + \ \frac{f_n - f_{n-1}}{ln(t_n/t_{n-1})} \ \frac{1}{s_f}\ E_1(s_f\ t_n) \tag{3.7}$$

The expression for $s_f\ \overline{f}(s_f)$ is straightforward. When working with real field data, which always contain a certain amount of noise, it is necessary to compute the last semilog slope $m = \frac{f_n - f_{n-1}}{ln(t_n/t_{n-1})}$ with an expression less sensitive to the last measurement, and a weighted logarithmic finite difference formula was used, which computes this slope on the last 0.2 or even 0.4 log-cycles. This is true as well for pressure as for flowrate measurements.

For a late time linear interpolation, the traditional Romboutsos and Stewart algorithm (1988) can be used:

$$\overline{f}(s_f) \ = \ \frac{f_0}{s_f} \ + \ \sum_{i=0}^{n-1} \ \frac{f_{i+1} - f_i}{t_{i+1} - t_i} \cdot \frac{e^{-s_f t_i} - e^{-s_f t_{i+1}}}{s_f^2} \ + \ \frac{f_n - f_{n-1}}{t_n - t_{n-1}} \cdot \frac{e^{-s_f t_n}}{s_f^2} \tag{3.8}$$

For a buildup, we can take a semilog interpolation with respect to Horner time:

$$\overline{f}(s_f) \ = \ \frac{f_0}{s_f} \ + \ \sum_{i=0}^{n-1} \ \frac{f_{i+1} - f_i}{t_{i+1} - t_i} \cdot \frac{e^{-s_f t_i} - e^{-s_f t_{i+1}}}{s_f^2} \tag{3.9}$$

$$+ \ \frac{f_n - f_{n-1}}{ln(\frac{t_n + t_p}{t_n} \frac{t_{n-1}}{t_{n-1} + t_p})} \cdot \frac{E_1(s_f(t_n + t_p)) \ - \ e^{-s_f t_p} E_1(s_f t_n)}{s_f} \tag{3.10}$$

We must be aware that the choice of the extrapolation is a crucial point of this study. The point is that a truncation problem arises if our data (pressure

measurements) stop before a given trend is set: what would the data would have looked like if the well test had lasted longer ? Would they have had a semilog behavior, or a linear behavior, or any other time dependance ? It is always disturbing to have to assume part of a result to get it, and following the feedback of numerous reviewers, we investigated a way to generalize our approach. Except for two cases, all the common models we work with in well testing show a log-derivative (often called derivative) that either stabilizes to a constant value (infinite acting radial flow), or displays a log-derivative with a constant slope on a log-log plot (1/2 for linear flow, -1/2 for spherical flow, or 1 for pseudo-steady state). The first exception is, of course, the buildup behavior, where the log-derivative continuously bends downwards. This can be remedied as in real space by rewriting the p_w vs. Δt file as a p_w vs. t_{eq} file:

$$t_{eq} = \Delta t \frac{t_p}{t_p + \Delta t} \tag{3.11}$$

t_{eq} is Agarwal's equivalent time (Ref. [20]), which can be generalized to any succession of buildups and drawdowns. The second exception is a constant pressure boundary, where the log-derivative bends downwards again. This case is not considered problematic either, since once the pressure does not move anymore (very small log-derivative, disappearing from the log-log plot), the extrapolation is not a problem any more. Before this stabilisation, the curved log-derivative can be approximated well enough with a straight-line on a log-log plot, and this extrapolation "sticks" to the data long enough (for the needed half-log cycle) so that, for $1/s_f < t_{max}$, the error can be neglected.

In all cases, this late time power extrapolation, as opposed to a linear or semilog extrapolation, seems to be general enough to "read" the needed information out of the data. It is necessary to get some second log-derivative information, which is computed by α. Let us denote $u = ln(t)$. Then the semilog slope at each point is: $f'(u) = \frac{df}{dln(t)}$. Instead of writing $f'(u) = f'(u_n) \equiv m$, we say that:

$$f'(u) = f'(u_n) \, (\frac{t}{t_n})^{\alpha} \quad \text{where} \quad \alpha = \frac{f''(u_n)}{f'(u_n)} \tag{3.12}$$

$$\text{integrating} \quad f(t) = f(t_n) + \frac{m}{\alpha t_n^{\alpha}}(t^{\alpha} - t_n^{\alpha}) \tag{3.13}$$

This can be integrated the following way:

$$\overline{f}(s_f) = \int_0^{t_n} f(t)e^{-s_f t}dt + \frac{m}{\alpha t_n^\alpha} \int_{t_n}^{\infty} (t^\alpha - t_n^\alpha)e^{-s_f t}dt \tag{3.14}$$

$$= \frac{f_0}{s_f} + \sum_{i=0}^{n-1} \frac{f_{i+1} - f_i}{t_{i+1} - t_i} \cdot \frac{e^{-s_f t_i} - e^{-s_f t_{i+1}}}{s_f^2} \tag{3.15}$$

$$+ \frac{m}{\alpha(s_f t_n)^\alpha} \frac{1}{s_f} \int_{s_f t_n}^{\infty} (x^\alpha - x_n^\alpha)e^{-x}dx \tag{3.16}$$

This last integration yields the incomplete Gamma function Γ, which can be accessed with the IMSL library for example, and which stands in our final algorithm **flapl8**, included in the Appendix:

$$\overline{f}(s_f) = \frac{f_0}{s_f} + \sum_{i=0}^{n-1} \frac{f_{i+1} - f_i}{t_{i+1} - t_i} \cdot \frac{e^{-s_f t_i} - e^{-s_f t_{i+1}}}{s_f^2} \tag{3.17}$$

$$+ \frac{m}{\alpha(s_f t_n)^\alpha} \frac{1}{s_f} \{ \Gamma(\alpha + 1, s_f t_n) - (s_f t_n)^\alpha e^{-s_f t_n} \} \tag{3.18}$$

If $\alpha \to 0$, this numerical Laplace transform reduces to Eqn. 3.7, which is easier to compute. We have visualized the effects of the different assumptions in Fig. 3.1. We performed the following test: we simulated some standard data, discretized them, took their Laplace transform, and came back to real space using Stehfest's algorithm (inverse Laplace transform, [5]). With perfect algorithms, the output should be the same as the input, for the function as well as for its derivative. We see in the first plot that this is not exactly true, if we use n=4 in Stehfest's algorithm. This means that there is a systematic error added in the process of taking the inverse Laplace transform. The error in the truncated data is larger due to a coarse estimate of the late time behavior of the data. On the second plot, the error is smaller due to a better accuracy in Stehfest's algorithm (n=6) during the storage transition. More importantly, the late time power extrapolation is much better for the truncated data, which is good news: we are able to overcome the lack of knowledge of the late time behavior of the pressure function to an extent which enables us to remain accurate in the pertinent time range.

In conclusion, we found an analytical expression which is general enough to treat all the usual late time behaviors, which is a significant improvement on what could be found in the literature until now.

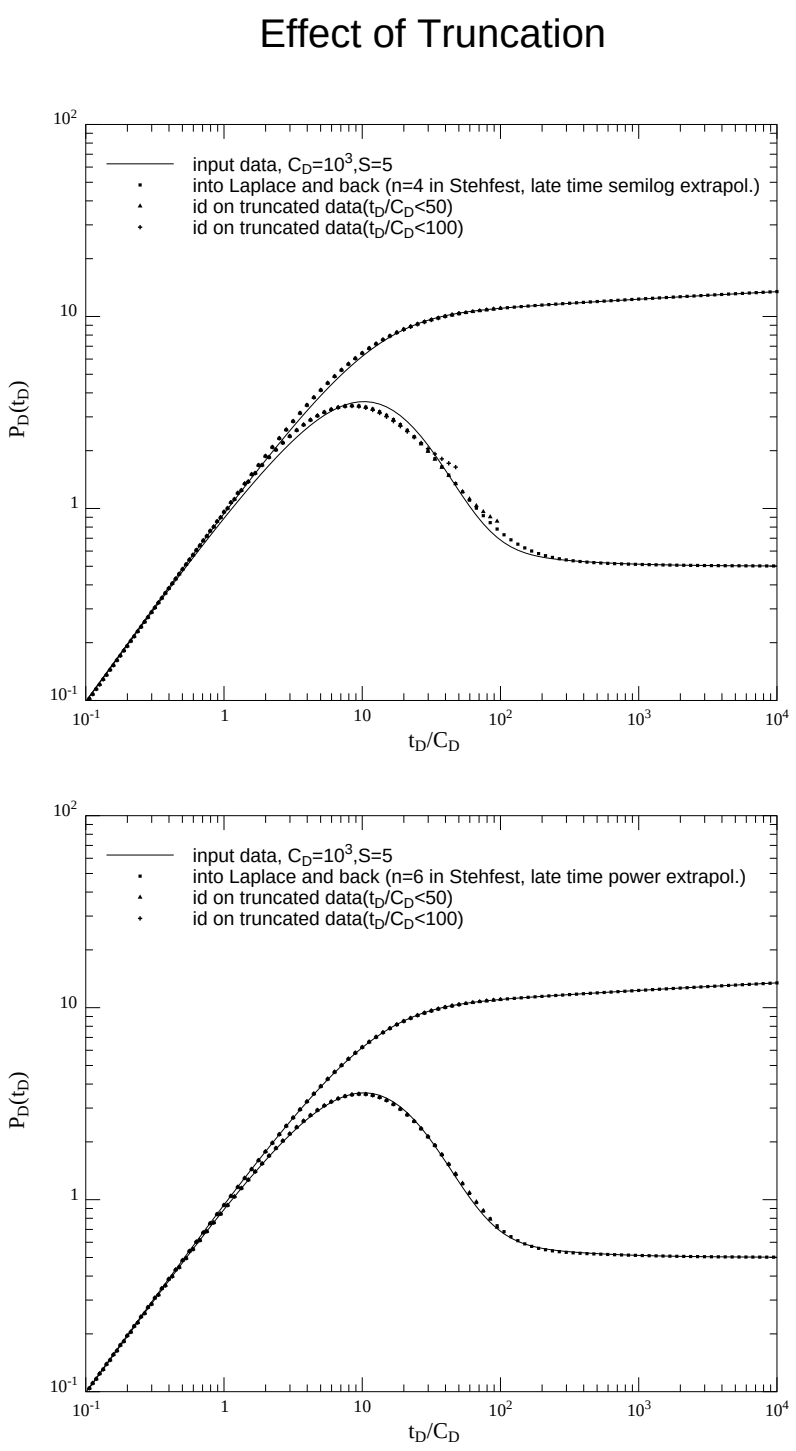

Figure 3.1: Verification of the formulae with Stehfest's algorithm

3.2 Type Curves

The application of the algorithm developed in the previous section makes it possible to take the Laplace transform of our data and to plot them in a representative and meaningful way. The next logical step is to plot type curves, since these have the advantage, in comparison to a traditional straight line analysis, to display not only the flow pattern when one single effect overwhelms all the rest, but also to show the transition zones between straight lines and to use them for matching. Given this, we have exactly the same requirements as in real space, which is highest possible resolution. Since we have shown already the similarity of behavior of both the real pressure and the Laplace pressure, we will be able to use the same sets of type curves. This will allow identification of the reservoir model and subsequent estimation of the unknown reservoir parameters.

The most useful type curves are not type curves for Kernel functions, but type curves which include wellbore storage and skin effects, as pointed out by Gringarten and Ramey [14, 15, 16].

Semilog plots have the strong advantage that they have constant resolution, because the early time pressure drop, which is very quick at the beginning, is plotted in a part of the curve where it is easy to see them. That is a well known advantage of a semilog plot that can be used for Laplace pressure as well. We can choose either $\log(s)$ or $\log(1/s)$ on the abscissa, since the results will be symmetric over a line parallel to the ordinate axis. For the sake of a familiar looking shape, we chose to work with the reciprocal Laplace variable $\frac{1}{s}$, as is shown in Figure 3.2. It is easy to see that when wellbore storage is present, the actual reservoir response is delayed, and that the presence of skin adds a dimensionless pressure drop which increases with the sandface flowrate, and stabilizes at the value of the skin factor.

A log-log plot can be used to shift the data horizontally and vertically until a good match is achieved. The Bourdet and al. [17] derivative type curves are the most useful, because the derivative is very characteristic, since it is located, thanks to its low value, in a part of the log-log plot where the resolution is high. What is good for real pressure is also good for Laplace pressure, and all we have to do is take the derivative Laplace quantities equivalent to those in real space and to plot them in a similar way. This

allows us to display a set of type curves in log-log scale as well, as shown in Figure 3.3. We plotted the Bourdet et al. type curve just below it to emphasize the similarity in behavior. These type curves are valid only for an infinite acting, homogeneous reservoir (with the usual assumptions that simplify the diffusivity equation). Since there is radial flow under these circumstances, the two parameters C_D and $skin$ (which we will note S) can be merged into $C_D e^{2S}$, which is an approximation we already know from real space, and which is valid as soon as the Kernel Function has a semilog behavior (with a 1/2 slope), which is the case for the time range $t_D > 30$. The only problem can be with very low values of $C_D e^{2S}$, where it becomes necessary to index the curves with both parameters C_D and S separately, however this is quite rare in practice. This problem exists in real space as well, as it is attribuable to the physics of the problem.

The log-derivative with respect to $1/s$ can be computed as follows:

$$\frac{d(s\overline{p_D}(s))}{dln(1/s)} = -s \frac{d(s\overline{p_D}(s))}{ds} \tag{3.19}$$

This derivative is smoother than in real space, because the Laplace pressure is still defined with an integral, and therefore the transitions in Laplace space are less abrupt than in real space. In this regard, the Laplace pressure derivative type curves are similar to the integral pressure type curves described by Reynolds and Blasingame.

$$\frac{\partial^2 p_D}{\partial r_D^2} + \frac{1}{r_D}\frac{\partial p_D}{\partial r_D} = \frac{\partial p_D}{\partial t_D} \tag{3.20}$$

$$\frac{\partial^2 \overline{p_D}}{\partial r_D^2} + \frac{1}{r_D}\frac{\partial \overline{p_D}}{\partial r_D} = s\ \overline{p_D}(s) - p_D(t_D = 0^+) \tag{3.21}$$

The arguments in favor of the Laplace space approach are that even when the real data are very noisy, the Laplace pressure and its derivative are still smooth, which makes it a very efficient diagnostic tool. Moreover, the better knowledge of the reservoir solutions in Laplace space and the fact that the treatment of flowrate variations is simplified, as shown in the following chapters, make the method more broadly useful in practice.

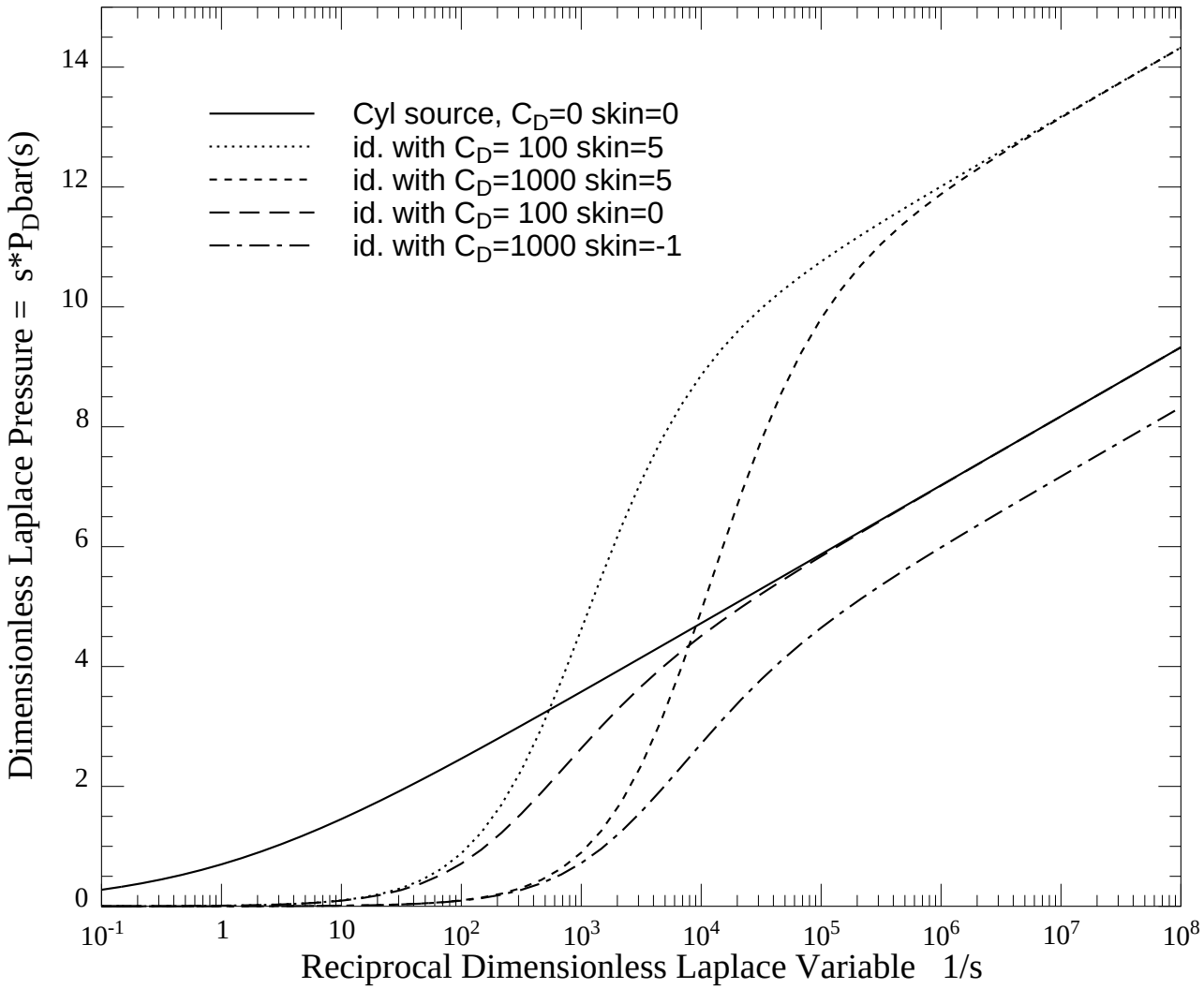

Figure 3.2: Effect of Wellbore Storage and Skin

One other useful advantage of Laplace space is that double porosity behavior can be taken into account very easily by replacing s by:

$$u \;=\; s\; f(s) \;=\; s\; \frac{\omega(1-\omega)s+\lambda}{(1-\omega)s+\lambda} \tag{3.22}$$

in the argument of the Bessel functions (Warren and Root, Ref. [18]). This holds for pseudosteady state interporosity flow, while for transient interporosity flow, the model suggested by deSwaan-O (Ref. [19]) can be used:

$$s\; f(s) \;=\; s\; (\; 1 \;+\; \sqrt{\frac{\lambda'\omega'}{3s}} tanh(\sqrt{\frac{3\omega' s}{\lambda'}})) \tag{3.23}$$

The definitions of λ' and ω' are given by:

$$\omega' = \frac{(\phi c_t h)_m}{(\phi c_t h)_f} \tag{3.24}$$

and

$$\lambda' = \frac{12L^2}{h_m^2}\frac{(kh)_m}{(kh)_f} \tag{3.25}$$

In Eqs. 3.24 and 3.25, h_m and h_f are the thickness of the individual matrix and fracture elements, respectively. The definition of the dimensionless time for this model is given by:

$$t_D = \frac{k_f t}{(\phi c_t)_f \mu L^2} \tag{3.26}$$

Type curves for pseudo steady state interporosity flow are shown in Figure 3.4. The first plot, which is in semilog scale, shows the Kernel function of the reservoir, which is the response if neither wellbore storage nor skin were present, and if the sandface flowrate had been a unit step function. For the second plot, which is in log-log scale, the more conventional case of a wellbore pressure including skin and wellbore storage is shown. The characteristic effects of ω and λ are the same as in real space, which is predictable considering the poperties of the Laplace pressure.

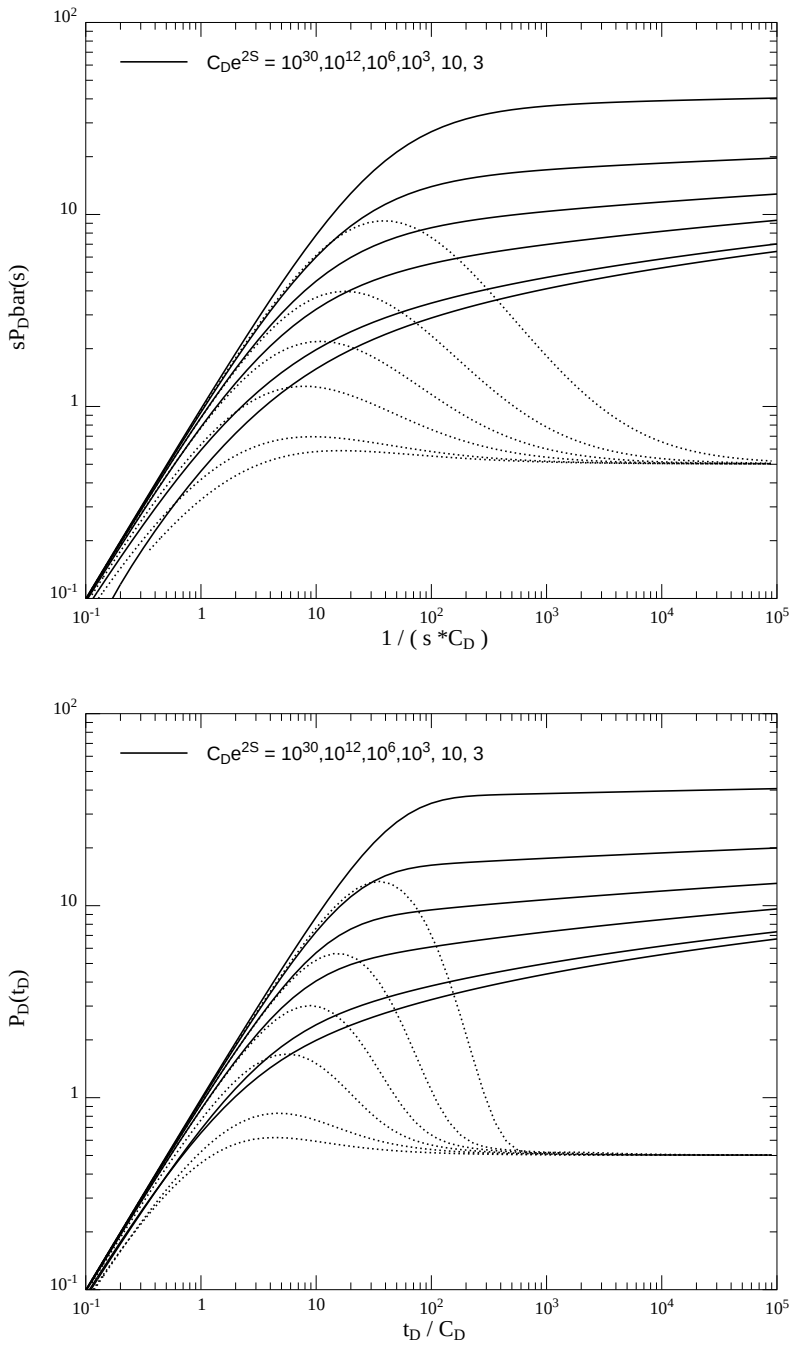

Figure 3.3: Derivative Type Curves

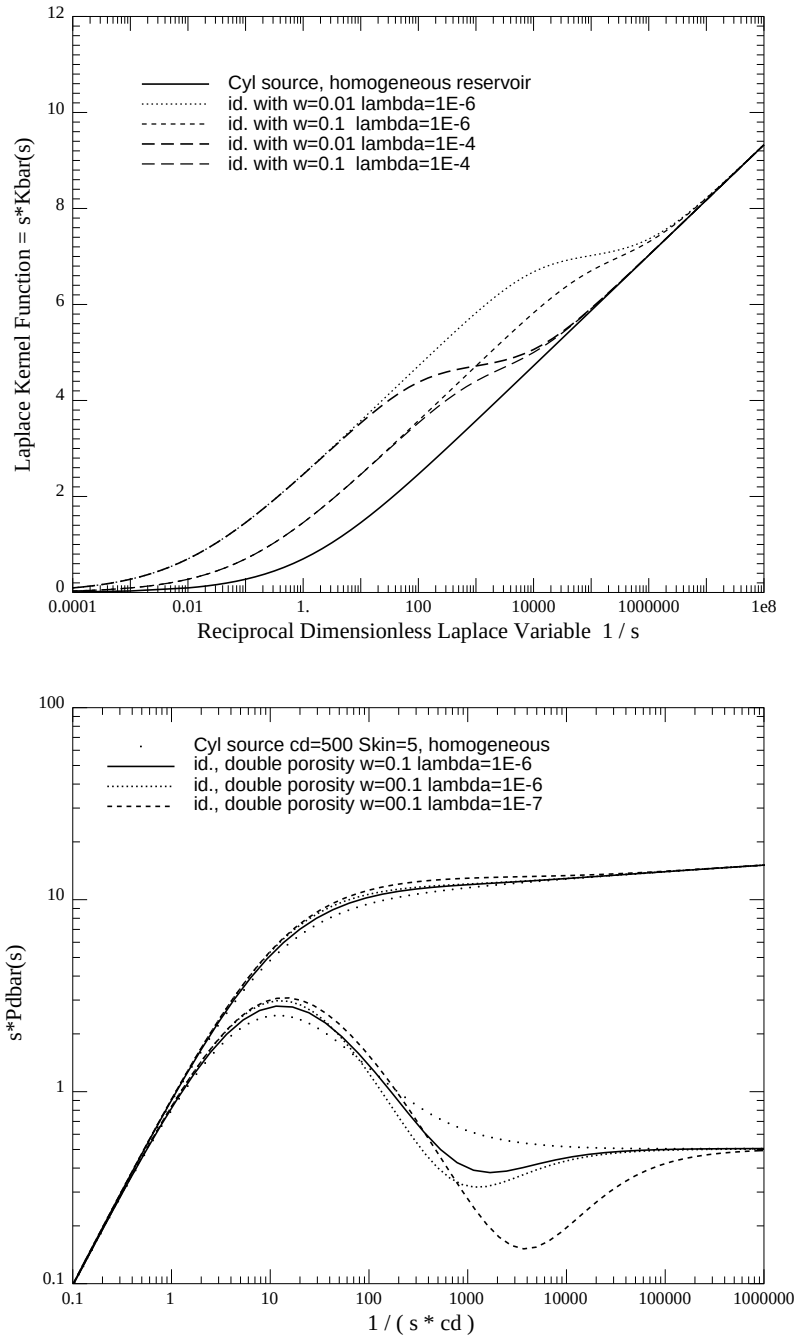

Figure 3.4: Effect of Storativity Contrast ω and Transfer Coefficient λ

Figure 3.5, shows the effect of partial penetration on the Kernel function. The plots do not include the effect of wellbore storage and skin due to damage at the wellbore. The first plot is in semilog scale, therefore the additional partial penetration skin is obvious. The values of this partial penetration skin are the same as if conventional real space plots had been used. In the second plot, which is log-log scale, different flow regimes are visible. At early time (that means at small $1/s$), the first radial flow is visible, with a Laplace pressure drop inversely proportionnal to the completion ratio. At middle times, we expect a -1/2 slope of the log-derivative in real space, but in Laplace space, since the transition is stretched, this spherical flow behavior is visible only for extremely small completion ratios ($h_w/h < 5\%$). The Kernel function has been computed for completion in the middle of the layer ($z_w = h/2$), for a homogeneous reservoir ($u = s$), using the following expression:

$$s\overline{K}(s) = K_0(r_D\sqrt{u}) + \frac{4}{\pi}\frac{h}{h_w}\sum_{n=1}^{\infty}\Big(\frac{1}{n}K_0(r_D\sqrt{u+\frac{n^2\pi^2}{h_D^2}}) \tag{3.27}$$

$$sin\ n\pi\frac{h_w}{2h}\ cos\ n\pi\frac{z_w}{h}\ cos\ n\pi\frac{z}{h}\ \Big) \tag{3.28}$$

Figure 3.6 shows the pressure drop in a well with wellbore storage and skin in a reservoir with a closed outer boundary. The linear pressure drop with respect to time gives a unit slope on a log-log plot, in Laplace space as well as in real space. The Kernel fuction has been computed with:

$$s\overline{K} = \frac{K_1(r_{eD}\sqrt{s})I_0(r_D\sqrt{s}) + I_1(r_{eD}\sqrt{s})K_0(r_D\sqrt{s})}{\sqrt{s}(I_1(r_{eD}\sqrt{s})K_1(\sqrt{s}) - I_1(\sqrt{s})K_1(r_{eD}\sqrt{s}))} \tag{3.29}$$

If $r_{eD} \gg 1$, this can be approximated as:

$$s\overline{K} = K_0(r_D\sqrt{s}) + \frac{K_1(r_{eD}\sqrt{s})I_0(r_D\sqrt{s})}{I_1(r_{eD}\sqrt{s})} \tag{3.30}$$

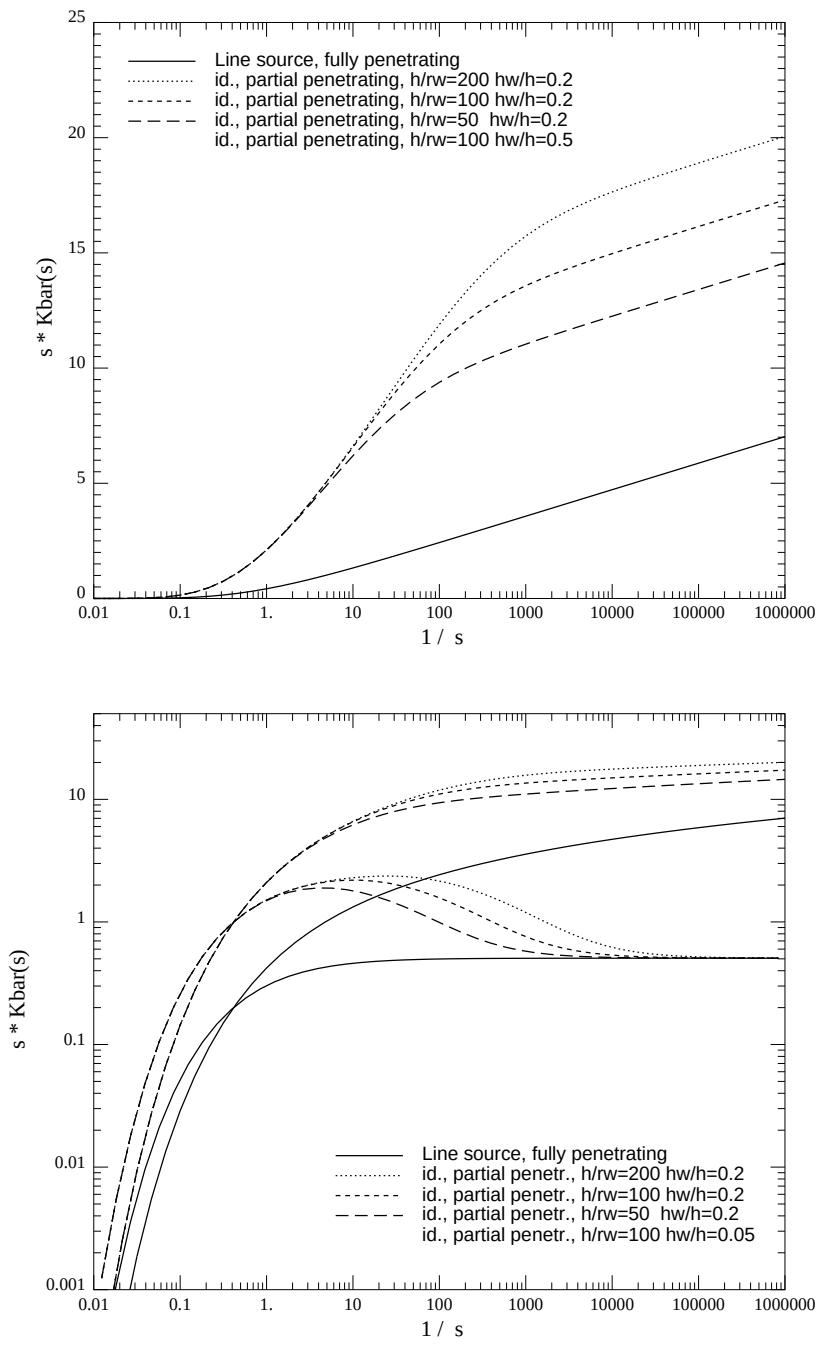

Figure 3.5: Effect Of Completion Ratio h_w/h On The Kernel Function

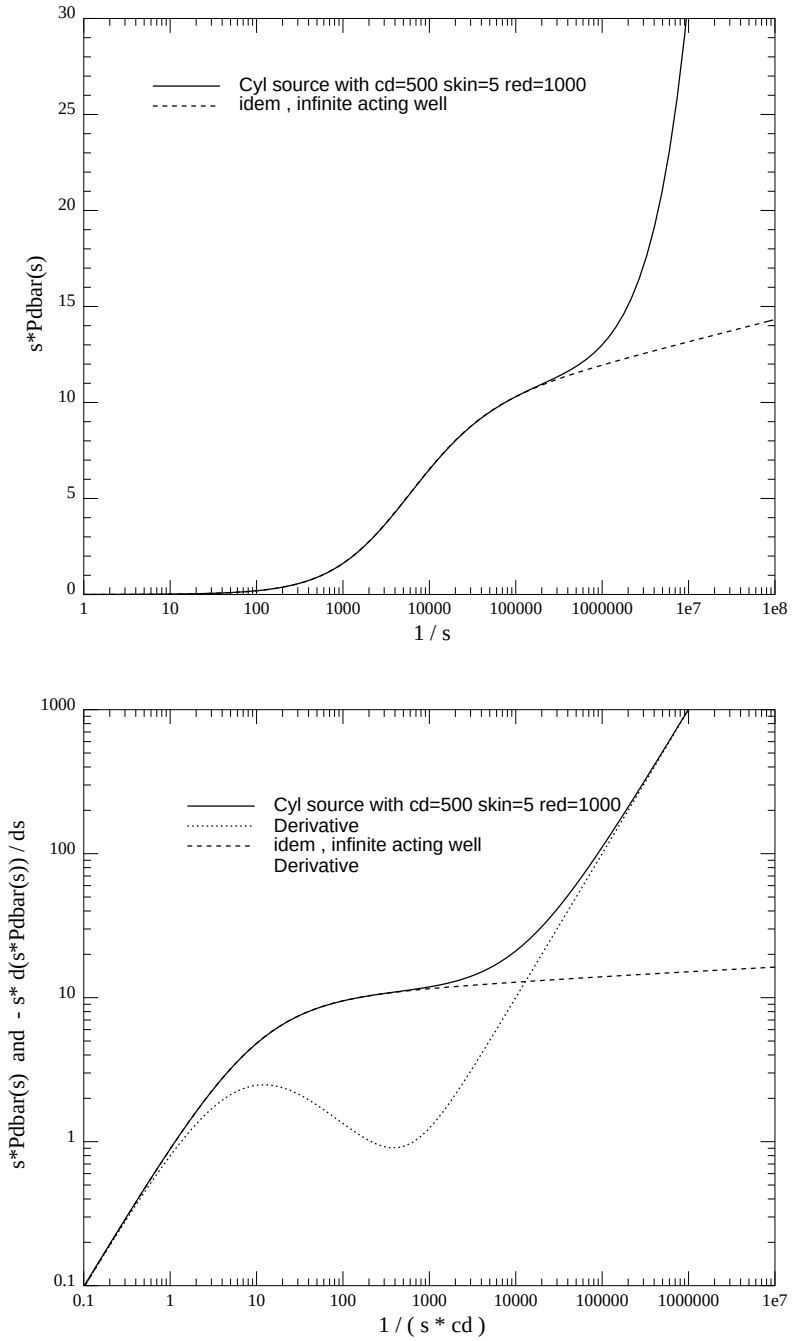

Figure 3.6: Linear Late Time Behavior For Bounded Reservoir

3.3 Treatment Of Wellhead Flowrate Variation

The previous section demonstrated that it was possible to generate characteristic type curves in Laplace space for any kind of problem using the solutions already published in the literature. However this is already possible in real space as well, although usually more time consuming, especially when infinite series have to be used for the computations. This section shows treatments for which the Laplace space approach brings substantial advantanges in comparison to the real space approach, using the background described in Section 2.2.

There are different kinds of deconvolution, depending on the physical origin of the flowrate variation and of the data available. If downhole flowrate measurements are available, wellbore storage deconvolution can be performed, as explained in Section 3.5. However in practice, there are other causes of flowrate variation than just wellbore unloading, and the most common is the fact that even at the wellhead, it is difficult to maintain the flowrate constant during the whole test. This can be due to change of the chokes, or by a slow cleaning-up of the well, or because the pump gets too weak when the pressure drop increases, or when light oils are evaporating, or many other reasons. The deconvolution treatment, namely dividing by the Laplace wellhead flowrate, is straightforward and stable:

$$s\ \overline{p_{wD_c}} \ = \ \frac{s\ \overline{p_{wD}}(s)}{s\ \overline{q_{wh_D}}(s)} \tag{3.31}$$

p_{wD_c} is the dimensionless wellbore pressure that we would have measured if the flowrate had been constant at the wellhead. It therefore includes wellbore storage and skin effect, since the boundary condition ($q_{wh_D} = 1$) is applied downstream of the wellbore. The advantage of this treatment is that the whole rate history can be used for the match, and not only the last time range where the flowrate is (supposed to be) stable. Thus, more information can be taken into account.

For the theoretical case where the flowrate is a step variation, the treatment is very simple, as it is in real space.

$$\text{If } t_D < 0 \quad q_{wh_D} = 0 \tag{3.32}$$

$$0 < t_D < t_{D1} \quad q_{wh_D} = q_1 \tag{3.33}$$

$$t_{D1} < t_D < t_{Dmax} \quad q_{wh_D} = q_2 \tag{3.34}$$

$$\text{Then } s\,\overline{q_{wh_D}} = q_1 + (q_2 - q_1)\, e^{-st_{D1}} \tag{3.35}$$

This treatment is very efficient and does not give any problems whatsoever, but can be made in real space as well. The advantage of the Laplace approach appears when the wellhead flowrate is not a succession of perfect step functions. The Laplace transform has to be taken numerically, and the deconvolution gives good results if the flowrate measurements are accurate enough.

As an example, consider the flowrate history displayed in Figure 3.7. The pressure data have been generated with 0.2 % random noise, using the superposition of the flowrate data. The model is a fully completed wellbore in a homogeneous reservoir ($k = 150mD,\ h = 35ft$), with a wellbore storage coefficient of $C = 0.006bbl/psi$, and a skin of $S = 1.3$. In addition, there is a sealing linear boundary, at a distance of $340ft$ from the wellbore.

A first match has been performed assuming that the flowrate was constant, which is certainly not true for the first 3 minutes. The production time is 72 hours. The match (first plot of Figure 3.8) gives erroneous results for all the parameters if the whole time range is considered, even though the flowrate looked almost perfect on the Cartesian plot. This emphasizes the importance of the early time data.

The second step took into account the variable wellhead flowrate. We took the Laplace transform of these data, and deconvolved the pressure data using Eq. 3.31. The results are plotted in Laplace space, using the appropriate variables $s_f\ \overline{p_w}(s_f)$ vs. $1/s_f$. The third plot of Figure 3.8 displays the deconvolved pressure and the match, after coming back to real space using Stehfest's algorithm. It can be seen that even though the data were somewhat noisy, the deconvolution is stable except for the first couple of points, and that it gives very good results for the parameter estimation.

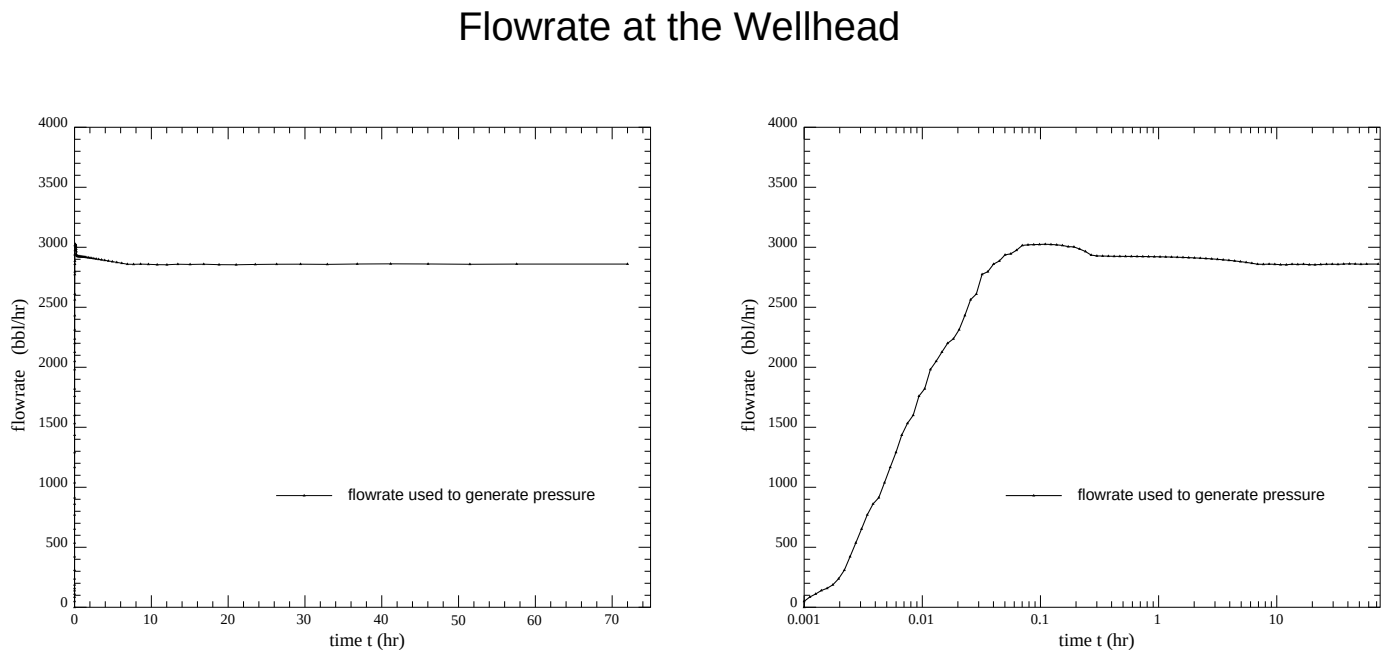

Figure 3.7: Cartesian and Semilog Plot Of Flowrate History

This highlights the importance of wellhead flowrate measurements, and demonstrates that drawdown data can be analysed successfully when q_{wh} is measured. The same is true, of course, if the measured flowrate is a downhole flowrate. This even shortens the storage transition period, and gives the best interpretation results. The only problem is that they are sometimes difficult to perform in practice, but recent improvements in downhole flowrate mesurement devices seem to be very encouraging in this regard. The field example in the Appendix shows a succesful application of this technique. It is not necessary to perform a costly buildup if the flowrate can be measured.

Figure 3.8: Deconvolution Of Wellhead Flowrate Variation

3.4 Buildup With No Measurement Prior To Shut-In

This section deals with an often encountered practical problem, which is that no measurements were made during the production time, and that only the pressure transient during the buildup was recorded. The procedure described here is equivalent to rewriting the buildup pressure file as a function of Agarwal's equivalent time (see Eq. 3.11, or Ref. [20]).

We know that buildup data do not behave like drawdown data, and therefore we cannot treat them in exactly the same way, especially when the duration of the test is not negligeable in comparison with the preceding production time. In real time, the solution is to use the "Horner" time, defined as:

$$t_H \;=\; \frac{t_p \;+\; \Delta t}{\Delta t} \tag{3.36}$$

If we denote as $p_{BU}(\Delta t)$ the buildup pressure with measurements starting at shut-in time ($\Delta t = 0$), we have in real space:

$$p_{BU}(\Delta t) \;=\; p_{DD}(\Delta t) \;-\; (\; p_{DD}(t_p + \Delta t) \;-\; p_{DD}(tp)\;) \tag{3.37}$$

If the initial drawdown has reached semilog behavior during the production time ($t \;<\; t_p$, with usually $b = 1/2$), we can derive:

$$p_{DD}(t_p + \Delta t) \;=\; a \;+\; b\; ln(t_p \;+\; \Delta t) \tag{3.38}$$

$$\rightarrow \quad \frac{dp_{BU}}{dln(t_H)} \;=\; -\frac{dp_{DD}(\Delta t)}{dln(\Delta t)} \;-\; \frac{\Delta t}{t_p}(\Delta t\; p'_{DD}(\Delta t) \;-\; b\;) \tag{3.39}$$

Therefore, as soon as $p_{DD}(\Delta t)$ reaches semilog behavior, the slope on the Horner plot is the same as the slope we would have had on a traditional plot for a drawdown test. The approximation is all the better if t_p is large.

We followed the same philosophy to find a Laplace variable which enables us to treat a builup test as a drawdown. Our new time variable will be Δt in the Laplace transform, and we define, with dimensionless variables:

$$\overline{p_{BU_D}}(s) \;=\; \int_{\Delta t_D=0}^{\infty} e^{-s\Delta t_D}\; p_{BU_D}(\Delta t_D)\; d\Delta t_D \tag{3.40}$$

Since we take the integral over the whole t_D range, the approximations must be valid over this whole range, and the only assumption we are making is that of Eq. 3.39. We find the same truncated integral that we found in Section 2.4, which yields an exponential integral:

$$s\;\overline{p_{BU_D}}(s) \;= s\;\overline{p_{DD_D}}(s) \;-\; b\;e^{st_{pD}}\;E_1(st_{pD}) \tag{3.41}$$

We have found a "Horner-like Laplace variable", which we call here s_{BU}, which has the required property: a $sp_{BU_D}(s)$ vs. s_{BU} plot has exactly the same shape as (it is identical to) a $sp_{DD_D}(s)$ vs. s plot. To do so we used the asymptotic behavior of the exponential integral, which can be found, although not over the whole x range at once, in Abramowitz's Handbook of Mathematical Functions (Ref. [21]):

$$-\,ln(x) - \gamma \;<\; e^x E_1(x) \;<\; \frac{1}{x} \tag{3.42}$$

For small x, the left-hand approximation is valid, and can be rewritten as $ln(1 + e^{-\gamma}/x)$, and when $x \to \infty$, the $1/x$ expression can be used, which we will rewrite as well as $ln(1 + 1/x)$. This can be summarized saying that:

$$e^x E_1(x) \;\simeq\; ln(1 + \frac{A(x)}{x}) \tag{3.43}$$

with $A(x)$ continuously increasing from:

$$lim_{x\to 0} A(x) \;=\; e^{-\gamma} \;\simeq\; 0.5614594835 \tag{3.44}$$

$$\text{to}\;\; lim_{x\to\infty} A(x) \;=\; 1 \tag{3.45}$$

We define the dimensionless buildup Laplace variable s_{BU} as:

$$s_{BU} \;=\; s \;+ \frac{A(s \cdot t_{pD})}{t_{pD}} \tag{3.46}$$

The full dimension buildup Laplace variable s_{BUf} is similarly:

$$s_{BUf} \;=\; s_f \;+ \frac{A(s_f \cdot t_p)}{t_p} \tag{3.47}$$

We derived a homographic approximation equating the two expressions in Eq. 3.43 for different values of x. Eq. 3.43 can then be used to compute the exponential integral for the whole positive x range (even for other purposes). The simplest is:

$$A(x) \;=\; \frac{x \;+\; 1.035e^{-\gamma}}{x \;+\; 1.035} \tag{3.48}$$

We prefer to work with a refined expression, which has a better fit:

$$A(x) \;=\; \frac{x^2 \;+\; 1.60718\; x \;+ 0.20025}{x^2 \;+\; 2.0908\; x \;+\; 0.35181} \tag{3.49}$$

Our buildup Laplace variable is therefore:

$$s_{BU} \;=\; s \;+\; \frac{1}{t_{pd}}\; \frac{(st_{pd})^2 \;+\; 1.60718\; (st_{pd}) \;+\; 0.20025}{(st_{pd})^2 \;+\; 2.0908\; (st_{pd}) \;+\; 0.35181} \tag{3.50}$$

We have plotted the results on Fig. 3.9. As in real space Horner plots, even though plotting $s\overline{p_D}(s)$ with respect to s_{BU} can distort the data when the assumptions to the treatment are not exact (no real semilog behavior), this is still an excellent diagnostic tool.

We investigated the case where there was only one producing time before the drawdown. In the case of a more complex flowrate history before the beginning of the pressure measurements, it is easier to use Agarwal's equivalent time and subsequently to take the Laplace transform of the p_w vs. t_{eq} file, than to try to generalize this result.

As a conclusion to this section, we have found a Laplace variable which is exactly equivalent to the Horner time in real space. We need the same assumptions as in real space (see Eq. 3.39) if we want to have a graph without distortion. The pressure buildup is all the bigger if the previous production time was long, so this appears as a constraint on our variable, as seen in Fig. 3.9.

$$\frac{\Delta t \;+ t_p}{\Delta t} \quad > \quad 1 \tag{3.51}$$

$$\text{is similar to} \qquad s_{BU} \quad > \quad \frac{e^{-\gamma}}{t_{pD}} \tag{3.52}$$

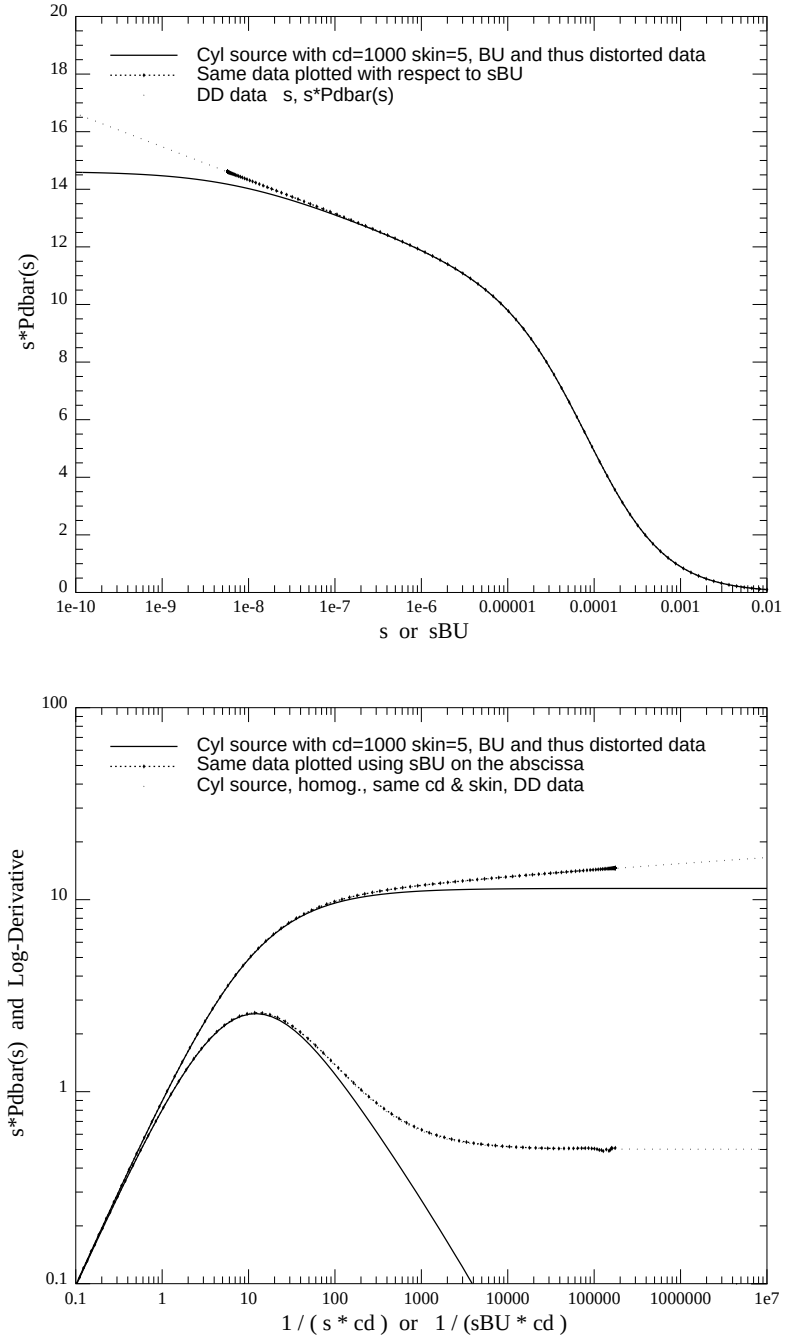

Figure 3.9: Example With Production Time Of $t_{pD} = 10^8$ and 2 10^5

3.5 Numerically Stable Wellbore Storage Removal

Since the effect of wellbore storage is to delay the flowrate impulse on the reservoir, removing the effect is a deconvolution process.

A lot of different deconvolution algorithms already exist, either using direct real space deconvolution, or curve-fitting approximations. The drawback of the former is that they are generally recursive, and therefore add up errors occuring in the first steps of the computation. The disadvantage of curve-fitting is that it is an approximation, and needs a lot of computation prior to deconvolution to find the best coefficients of each function. A way to avoid this problem is to constrain the deconvolved pressure to stabilize it, but this requires additional computation time as well.

The advantage of our Laplace space approach is that it does not have this stability problem due to recursivity, because the Laplace transform takes the whole time range into account. The only stability problem we encountered was at early times, for wellbore storage deconvolution. This can be handled by removing the wellbore storage only partially, as will be shown in this section. We must be aware of the fact that when the formulas of Section 2.2 are used with no downhole flowrate measurements, we have to estimate the sandface flowrate as:

$$s\ \overline{q_{sf_D}}(s) \ = \ 1 \ - \ C_D s^2 \overline{p_{wD}}(s) \tag{3.53}$$

This formula looks interesting, because we do not need to know kh to compute it, since $\alpha_p = \alpha_t / \alpha_C$. However using this formula, deconvolution is unstable numerically. This means that the slightest noise, or a small inaccuracy of our C estimate, or the fact that the physical wellbore storage is not constant, make this treatment impossible in practice. This is understandable because the time derivative of the cylindrical source function tends to infinity at early time, and therefore creates a singularity in the convolution integral. This is why if deconvolution has to be performed, the flowrate used

should not be the sandface flowrate, but the flowrate just above the perforations, which we will call q_m, because this is the flowrate measured when a bottomhole flowmeter is installed. This has the advantage that there is the small remaining storage of the rathole, or of the small volume of the wellbore under the flowmeter, which will stabilize the deconvolution. We will call C_r this residual storage, and p_{wc} the deconvolved pressure . p_{wc} is the measured pressure drop if the bottomhole flowrate is a unit step:

$$q_{mD} = 1 \quad \text{if} \quad t > 0 \tag{3.54}$$

Actually, with this assumption, the sandface flowrate at early times is smaller than unity, and the following mass balances can be written, assuming constant wellbore storage:

$$q_{sfD} = q_{whD} - C_D \frac{dp_{wD}}{dt_D} \tag{3.55}$$

$$q_{mD} = q_{whD} - (C - C_r)_D \frac{dp_{wD}}{dt_D} \tag{3.56}$$

Since the diffusivity equation is linear, the pressure drops remain proportional to the flowrate, and thus:

$$s\ \overline{p_{wD}}(s) = s\ \overline{q_{mD}}(s)\ \cdot s\ \overline{p_{wDc}}(s) \tag{3.57}$$

This relation is exact, even if the wellbore storage is changing or if p_w was measured with a non-step wellhead flowrate. This shows how much information bottom-hole flowrate measurements contain. In the simpler case where p_w corresponds to a constant wellhead flowrate, the algebra to deconvolve the pressure without flowrate measurements is the following:

$$s\ \overline{p_{wDc}}(s) = \frac{s\ \overline{p_{wD}}(s)}{1 - (C - C_r)_D\ s^2\ \overline{p_{wD}}(s)} \tag{3.58}$$

This procedure has been tested on an example where a large wellbore storage was hiding the early time behavior of the test, and deconvolution removed the ambiguity by displaying an early time double porosity behavior. This example is a 96 hour drawdown test, with simulated pressure data, to which we have added 0.2 % noise. The model used was a reservoir with pseudo-steady state double porosity behavior ($\omega = 0.05$ and $\lambda = 2\ 10^{-7}$),

with an impermeable linear boundary at a distance of $r_{bdry} = 300ft$ to the wellbore. The other parameter values are: $k = 200mD$, $S = 1.5$, and $C = 0.1bbl/psi$. The wellhead flowrate was constant $q = 2500bbl/day$. For the sake of completeness, the other parameters were: $\phi = 0.2$, $\mu = 1cP$, $B = 1.2$, $h = 15ft$, $c_t = 8\ 10^{-6}/psi$, and $r_w = 0.3ft$.

We matched these $p_w(t)$ vs. t data using a simple infinite-acting radial flow model, with nonlinear regression (also known as automated type curve matching), and we obtained the match of the first plot of Fig. 3.10. The confidence intervals were quite low, but the results were <u>not</u> correct. This misinterpretation is due to a wrong model choice, and it is impossible to perform the proper model identification without deconvolving (or having other information).

To deconvolve these data, we needed measurements of the downhole flowrate. The flowrate above the perforations was computed using Eq. 3.56, with a rathole storage of $C_r = 1.5\%\ of\ C$. We added 2 % noise to these q_m data for the first 6 minutes, and then 0.5 % noise until the end of the test. We performed the devonvolution using the same algorithm as in section 3.3. After deconvolution, the early time behavior is much more visible because the huge wellbore storage is removed to 98.5 %, and it is clearly evident on a log-log plot of p_{wc} that there is a double porosity behavior for the reservoir, and that there must be a boundary effect after 2 to 3 hours. We then performed the matching on the deconvolved data using the exact model. This is displayed in the second plot of Fig. 3.10. It can be seen that this interpretation gives much better results than the first one. Nevertheless, the skin is still quite poorly determined, as is r_{bdry}. ω and λ are poorly determined as well, but this is nearly always the case.

Figure 3.10: Matching With Wrong Model, Then Deconvolution, Then Matching With Proper Model

The imprecision on the value of the skin is understandable since we know that the skin is mostly determined by the wellbore storage transition. If we work with deconvolved data, the range of the pressure response is much smaller (we start with a bigger pressure drop) than for conventional data. Nonetheless, deconvolution has allowed us to find the right model.

It was known in advance that it is better to perform matching on the original variable rate data, since information is lost during the deconvolution process. So, using the deconvolved data only as a means to recognize the reservoir model, we then went back to the $p_w(t)$ vs. t data, and performed the parameter estimation using the proper double porosity, impermeable linear boundary model. The results are summarized on the last plot of Fig. 3.10, and it can be seen that this matching gives better results than with the deconvolved data (second plot), again except for ω and λ.

If we generalize these results, we can say that deconvolution allows us to perform a good model identification, and that the final match is the most effective on non-deconvolved, traditional $p_w(t)$ vs. t data. This can be explained by the fact that if our impulse q is more complicated, it will give us more information on the reservoir response p_w.

As a conclusion to this section, wellbore storage deconvolution should never be performed using the whole storage, but must leave a residual storage to stabilize the treatment. If good downhole measurements are available, deconvolution can be applied to perform model recognition, and if the data are very good, it even allows parameter estimation on the deconvolved pressure. If the flowrate data are very noisy so that the computation of the deconvolved pressure is impossible in real space, we can still examine the deconvolved pressure in Laplace space, which is more stable, and still recognizable. For this analysis, the type curves in Laplace space can be used to recognize the shapes.

Therefore, as soon as the flowrate, or in a less favorable situation the storage, are measured with a satisfying accuracy, model identification can be performed using wellbore storage removal in Laplace space.

3.6 Pressure Dependant Wellbore Storage

In the previous section, the wellbore storage was assumed constant in time. However we know that this is only a coarse assumption, since the compressibility of the fluids in the annulus is a function of pressure and temperature. Therefore, if a well test has a big pressure drop, the absolute pressure $p_w = p_{w0} + \Delta p_w$ becomes important. We made the assumption that the compressibility of the fluids, and thus the wellbore storage as well, was inversely proportionnal to the absolute pressure. With dimensionless variables, we denote in this section:

$$p_{wD} = p_{wD0} + \Delta p_{wD} \tag{3.59}$$

$$C_D = C_{D0} \frac{p_{wD0}}{p_{wD}} \tag{3.60}$$

Let us assume that we are using the results of the last section, and that we only want to remove part of the wellbore storage, for example $\beta = 90\%$. This means $C - C_r = \beta C$. The flowrate conservation equation still holds as:

$$q_{mD} = 1 - \beta\, C_D \frac{dp_{wD}}{dt_D} \tag{3.61}$$

The resulting Laplace flowrate can be computed as:

$$s\, \overline{q_{mD}}(s) = 1 - \beta\, C_{D0}\, p_{wD0} \int_0^\infty e^{-st_D} \frac{dp_{wD}(t_D)}{p_{wD}(t_D) dt_D} dt_D \tag{3.62}$$

$$= 1 - \beta\, C_{D0}\, p_{wD0}\, L\{\frac{d\ ln(p_{wD}(t_D))}{dt_D}\} \tag{3.63}$$

$$= 1 - \beta\, C_{D0}\, p_{wD0}\, \{s\, \overline{ln(p_{wD}(t_D))} - ln(p_{wD0})\} \tag{3.64}$$

$$= 1 - \beta\, C_{D0}\, p_{wD0}\, s\, \overline{ln(\frac{\Delta p_{wD} + p_{wD0}}{p_{wD0}})}(s) \tag{3.65}$$

The deconvolved pressure drop (or increment) can then be computed as:

$$s\ \overline{\Delta p_{wDc}}(s) = \frac{s\ \overline{\Delta p_{wD}}(s)}{s\ \overline{q_{mD}}(s)} \tag{3.66}$$

$$= \frac{s\ \overline{\Delta p_{wD}}(s)}{1\ -\ \beta\ C_{D0}\ p_{wD0}\ s\ \overline{ln(\frac{\Delta p_{wD}+p_{wD0}}{p_{wD0}})}(s)} \tag{3.67}$$

To our knowledge, this expression is new as well. It may look unusual, but it can be used with dimensional quantities, and this treatment can thus be performed with only an estimate of the initial wellbore storage C_0, which is easily accessible. The absolute pressure p_{w0} at the beginning of the test can be measured as well as the pressure drop, and we can write:

$$s_f\ \overline{\Delta p_{wc}}(s_f) = \frac{s_f\ \overline{\Delta p_w}(s_f)}{s_f\ \overline{q_m}(s_f)} \tag{3.68}$$

$$= \frac{s_f\ \overline{\Delta p_w}(s_f)}{1\ -\ \beta\ C_0\ p_{w0}\ s_f\ \overline{ln(\frac{\Delta p_w+p_{w0}}{p_{w0}})}(s_f)} \tag{3.69}$$

Again, since we have the data and the algorithm to take the Laplace transform, nothing hinders us to perform this treatment, except the fact that we never did it before. We tested this approach on the example plotted on Fig. 3.11, which is a builup test from Alaska. The long lasting storage transition and the important pressure increment made this test interesting for our purpose. After wellbore storage removal, we were able to recognize a radial composite model, which is in accordance with the fact that gas has been injected around this well and therefore created a higher mobility zone at some distance.

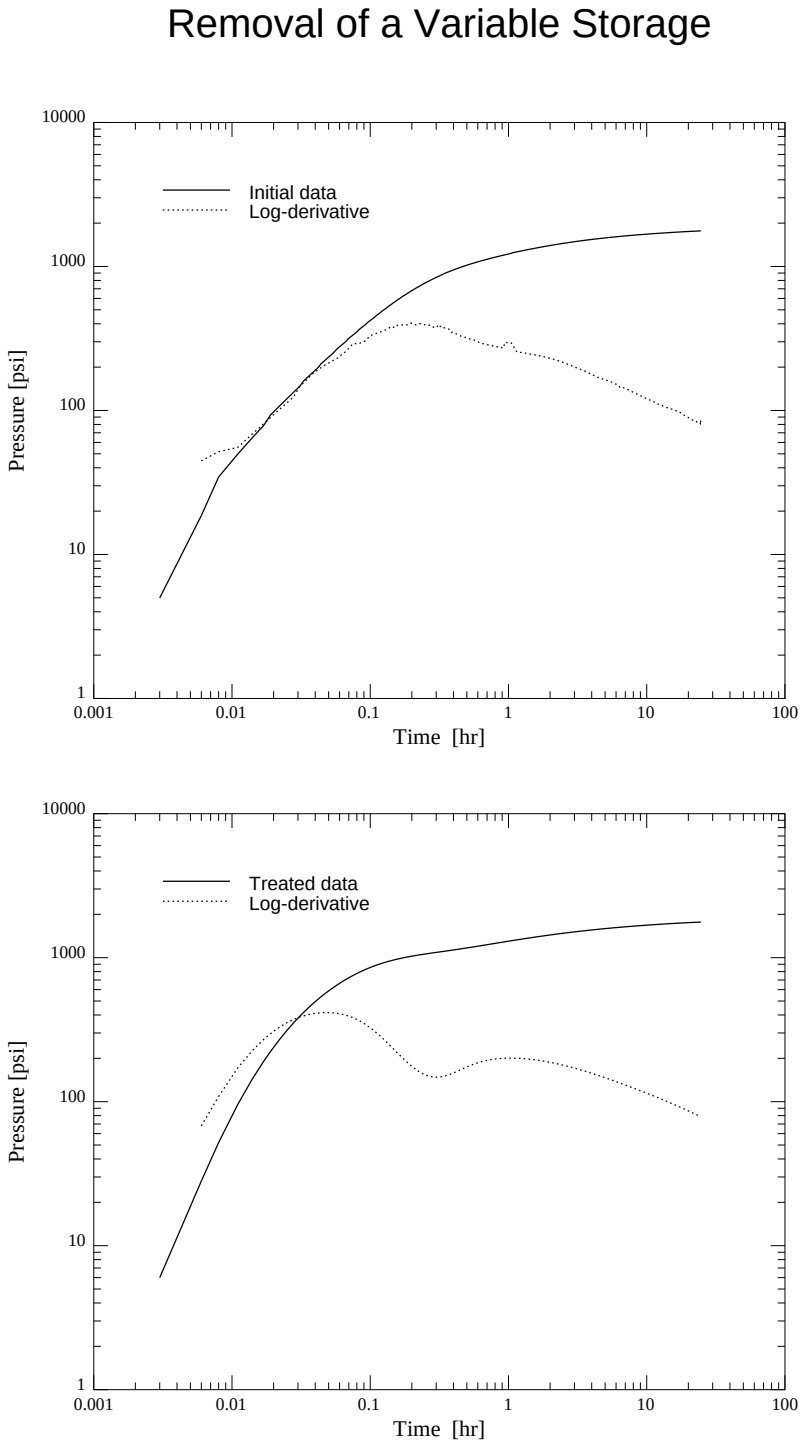

Figure 3.11: Application to Real Field Data (Buildup)

3.7 Nonlinear Regression in Laplace Space

Much of the parameter estimation in well test analysis today is performed with automated type-curve matching, which amounts to a nonlinear regression to minimize the difference between the data and the chosen model. This final step of the analysis has to be done once a model is chosen, and we have seen previously some additional tools to perform model recognition. In particular, removing the wellbore storage can unveil some early-time behavior indicative of a particular well or reservoir model. Usually, if we denote as ndp the number of (pressure) data points, and $\vec{\alpha} = (k, C, S, ...)$ the variable vector which contains permeability, storage, skin and any other parameter defined in the model, the problem can be formalized as follows:

$$Min_{\vec{\alpha}} \ \Sigma_{i=1}^{ndp} [\ p_{model}(t_i, \vec{\alpha}) \ - \ p_{measured}(t_i)\ ]^2 \tag{3.70}$$

Most models are known in Laplace space ([2, 3]), and therefore each computation of $p_{model}(t, \vec{\alpha})$ requires the use of a numerical inverter ([4, 5]). Typically with Stehfest's algorithm, the computation of one point in real space requires 6 or 8 computations in Laplace space. This is all the more time-consuming as these computations may be expensive if infinite sums occur. This problem is further aggravated if numerous iterations (up to 10 or 20) have to be performed before convergence. Based on the work showed in this study, we thought that we could choose a range for the Laplace variable, where the Laplace pressure would convey as much information as the real pressure itself. Logically, we chose ndp points , with $1/s_{f_i} = \ t_i, \ i = 1..ndp$. The regression was performed using a least-square problem as well:

$$Min_{\vec{\alpha}} \ \Sigma_{i=1}^{ndp} [\ s_{f_i}\ \overline{p_{model}}(s_{f_i}, \vec{\alpha}) \ - \ s_{f_i}\ \overline{p_{measured}}(s_{f_i})\ ]^2 \tag{3.71}$$

Of course, the parameter vector $\vec{\alpha}$ is exactly the same as in the previous equation. The first term of the square bracket is easier to compute than previously, since it is computed directly in Laplace space. The second term requires the application of a Laplace transform algorithm to the measured data, for example flapl8 listed in the Appendix. The advantage is that this

second term has to be computed only once, and does not change any more as $\vec{\alpha}$ is updated during the regression.

A Gauss-Newton minimization was performed using this approach. The data were taken from the example treated in Fig. 3.10. We did the regression assuming a standard infinite acting, storage and skin model. The real space regression algorithm converged in 8 iterations. With the same starting point, our Laplace space algorithm converged to the same solution (within 1 %) in 6 iterations. The search path is shown in Fig. 3.12. The main difference is not the number of iterations, but the fact that the regression requires less computations for each iteration. The fact that the objective function is smoother in Laplace space is only of slight advantage here. It would have been more important if the data had been noisier. For example, it would probably still be possible to match on the derivative in Laplace space, whereas we would have to match on the pressure itself in real space, if the data were very noisy. Another advantage of the regression in Laplace space is of course when the flowrate is varying during the test. Typically, if a downhole flowrate q_m is measured, the regression can be performed directly on:

$$s_f \, \overline{\Delta p_w}(s_f) \;=\; s_f \, \overline{\Delta p_{wc}}(s_f) \;\cdot\; s_f \, \overline{q_m}(s_f) \tag{3.72}$$

In such a case, regression in real space on $p_w(t)$ would require either a tedious superposition of $p_w c(t)$ [10], or an inversion of Eq. 3.72 with Stehfest's algorithm for example [4, 5]. If Laplace space has to be used on the data anyway for deconvolution, and since we usually have to use it for the model, it seems logical to use it for the regression as well.

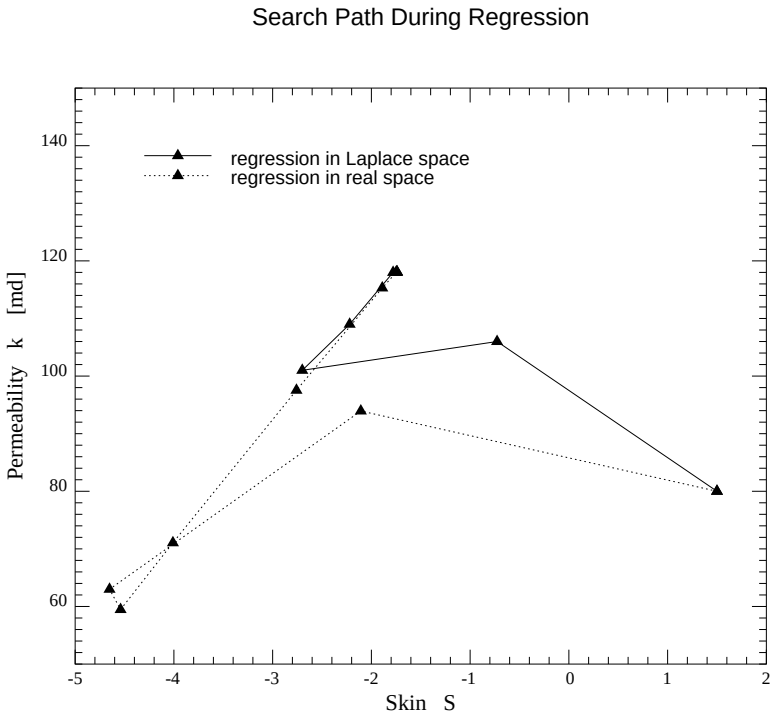

Figure 3.12: Nonlinear Regression in Laplace Space and Real Space

Chapter 4

Conclusion

The following findings were obtained from this study:

(1) The Laplace transform can be displayed in a characteristic, familiar looking way if the variables s_f $\overline{p_w}(s_f)$ vs. $1/s_f$ are chosen. These variables have the same dimension as $p_w(t)$ vs. t.

(2) Taking these variables, or the equivalent dimensionless expressions s $\overline{p_{wD}}(s)$ vs. $1/s$, it is possible to plot type curves in Laplace space with the same log-derivative as in real space. These type curves are smoother than in real space, but still characteristic enough to perform model identification. If implemented in an automated type curve matching procedure, they allow the whole parameter estimation to be performed in Laplace space, since the Laplace transform contains as much information as its original function in real space.

(3) Although we need to know the behavior of the function (usually $p_w(t)$) over the whole time range, we have seen that a linear interpolation at early time and a power extrapolation at late time, with first and second derivative information, are satisfactory for the computation of the Laplace transform. We developed adequate algorithms for this purpose, and tested them successfully on simulated as well as on actual field data.

(4) We have found a Laplace variable s_{BU} which is similar to Horner time, and allows us to treat buildup tests like a drawdown, even with no measurements prior to shut-in. The assumptions we need are the same as for the Horner variable, namely that the preceeding production time was long enough to have reached a semilog behavior.

(5) Our Laplace space approach is the natural approach if deconvolution has to be performed. In practice, if flowrate measurements are available, the model must be recognized using either real space or Laplace space type curves, but always dividing the Laplace pressure by the Laplace flowrate. If the quality of the data is good enough, final match can be obtained on the deconvolved data, but the best results are usually found matching the measured pressure data taking into account the flowrate history with superposition.

(6) For wellbore storage deconvolution without flowrate measurements, which is the less favorable case, the same procedure can be applied, simply estimating the flowrate from the storage and the pressure derivative. A residual storage should be left to stabilize that treatment. The storage does not need to be assumed constant for this treatment.

(7) Nonlinear regression can be performed in Laplace space, and this has been done successfully. The regression is computationally more efficient, by at least a factor of six or eight, depending on the value of the Stehfest parameter. The Laplace space regression also offers advantages if the data are noisy.

This approach provides an entirely new way of examining and understanding well test results.

4.1 Nomenclature

b	=	semilog slope
c_t	=	total compressibility, psi^{-1}
C	=	wellbore storage constant, bbl/psi
f	=	time fuction
h	=	formation thickness, ft
k	=	permeability, md
n	=	number of available data points
p	=	pressure, psi
q	=	flowrate, B/D
r	=	radius, ft
s	=	Laplace variable (dimensionless)
s_f	=	fully dimensional Laplace variable, hr^{-1}
S	=	damage skin
t	=	time, hr
μ	=	oil viscosity, cp
τ	=	dummy integration variable
ϕ	=	system porosity
ω	=	storativity contrast in fissured reservoirs
λ	=	transfer coefficient in fissured reservoirs

4.2 Subscripts and Superscripts

D	=	dimensionless
H	=	Horner time
c	=	constant rate = deconvolved
sf	=	sandface
wh	=	wellhead
m	=	measured or at the flowmeter
r	=	residual
w	=	well, wellbore or perforated
$'$	=	time derivative of
$\overline{f}$	=	Laplace transform of f

Bibliography

[1] van Everdingen, A.F. and Hurst, W.: "The Application of the Laplace Transformation to Flow Problems in Reservoirs", *Trans.*, AIME (1949)186, 305-324.

[2] Ozkan, E. and Raghavan, R.: "Some New Solutions to Solve Problems in Well Test Analysis: Part 1 - Analytical Considerations", SPE 18165, 1989.

[3] Ozkan, E. and Raghavan, R.: "Some New Solutions to Solve Problems in Well Test Analysis: Part 2 -Computational Considerations and Applications", Nov. 1989.

[4] Crump, K.S.: "Numerical Inversion of Laplace Transforms Using a Fourier Series Approximation", *Journal of the ACM*, Jan. 1976, Vol. 23, 89-96.

[5] Stehfest, H.: "Numerical Inversion of Laplace Transforms", *Communication of the ACM*, Jan. 1970, Vol. 13, No.1, 47-49.

[6] Rosa, A.J. and Horne, R.N.: "Automated Type-Curve Matching in Well Test Analysis by Using Laplace Space Determination of Parameter Gradients", paper 12131 presented at the 1983 SPE Annual Technical Conference and Exhibition, San Francisco, Sept. 5-8.

[7] Kuchuk, F.J., Carter, R.G. and Ayestaran, L.: "Numerical Deconvolution of Wellbore Pressure and Flow Rate", SPE 13960, 1985.

[8] Kuchuk, F.J.: "Applications of Convolution and Deconvolution to Transient Well Tests", *SPEFE*, Dec. 1990.

[9] Chaumet, P., Pouille, J. and Séguier, P.: "Application de la transformation de Laplace à l'étude des courbes de pression en régime transitoire", *Revue de l'Institut Français du Pétrole*, Dec. 1962.

[10] Guillot, A.Y. and Horne, R.N.: "Using Simultaneous Downhole Flow Rate and Pressure Measurements To Improve Analysis of Well Tests", *SPEFE*, June 1986, 217-26.

[11] Romboutsos, A. and Stewart, G.: "A Direct Deconvolution or Convolution Algorithm for Well Test Analysis", paper SPE 18157 presented at the 63rd SPE Annual Technical Conference and Exhibition, Houston, TX, Oct. 2-5, 1988.

[12] Earlougher, R.C. Jr. and Kersch, K.M.: "Analysis of Short-Time Transient Test Data by Type-Curve Matching", *JPT*, July 1974, 793-800; *Trans.*, AIME, 257.

[13] Gringarten, A.C.: "Type-Curve Analysis: What It Can Do and Cannot Do", paper SPE 16388, *JPT*, Jan. 1987, 11-13.

[14] Gringarten, A.C. et al.: "A Comparison Between Different Skin and Wellbore Storage Type-Curves for Early-Time Transient Analysis", paper SPE 8205 presented at the 1979 SPE Annual Technical Conference and Exhibition, Las Vegas, Sept. 23-26.

[15] Ramey, H.J., Jr. and Agarwal, R.G.: "Annulus Unloading Rates as Influenced by Wellbore Storage and Skin Effect", *SPEJ*, Oct. 1972, 453-62.

[16] Ramey, H.J. Jr.: "Short-Time Well Test Data Interpretation in the Presence of Skin Effect and Wellbore Storage", *JPT*, Jan. 1970, 97-104; Trans., AIME, 257.

[17] Bourdet, D. et al: "A New Set of Type Curves Simplifies Well Test Analysis", *World Oil*, May 1983, 95-106.

[18] Warren, J.E. and Root, P.J.: "The Behavior of Naturally Fractured Reservoirs", *SPEJ*, Sept. 1963, 245-255.

[19] deSwaan - 0, A.: "Analytical Solutions for Determining Naturally Fractured Reservoir Properties by Well Testing", *SPEJ*, June 1960, 117-122.

[20] Agarwal, R.G.: "A New Method to Account for Producing TIme Effects When Drawdown Type Curves are Used to Analyse Pressure Buildup and Other Test Data", paper SPE 9289 presented at the 55th SPE Annual Technical Conference and Exhibition, Dallas, TX, Sept 21-24, 1980.

[21] Abramowitz, M. and Stegun, I.A.: "Handbook of Mathematical Functions", Dover Publications, Inc., New York (1972)

[22] Meunier, D.F., Wittman. M.J. and Stewart, G.: "Interpretation of Pressure Buildup Test Using In-Situ Measurement of Afterflow", *JPT*, Jan. 1985, 143-52.

Chapter 5

Appendix

5.1 Fortran Program

```
      real*8 function flapl8(s,pd,td,ndp,pinitl)
c - written by Marcel Bourgeois, Nov 1991
c - takes the Laplace transform of a (p,t) file written as array
c - can be used for pressure or flowrate, dimensionless or not
c expin= exponential integral, DGAMIC= incomplete Gamma function
c
      IMPLICIT real*8 (a-h, o-z)
      dimension pd(400), td(400)
c - computation of last semilog slope on 0.1 or 0.2 log cycle
      nstep = 2
      if (nstep.eq.1) width=0.2
      if (nstep.eq.2) width=0.1
      if (nstep.eq.3) width=0.05
      do 60 ii=ndp-1, 2, -1
            if (dlog(td(ndp)/td(ii)).ge.width) then
            i=ii
            goto 62
            endif
 60   continue
 62   do 65 kk=i-1, 1, -1
            if (dlog(td(i)/td(kk)).ge.width) then
            k=kk
            goto 67
            endif
 65   continue
c ----- left log derivative -----
 67    m = dlog(td(ndp)/td(i)) * pd(k)
     & / ( dlog(td(i)/td(k)) * dlog(td(ndp)/td(k)) )
     & + dlog( td(ndp)*td(ndp)/(td(i)*td(k)) ) * pd(ndp)
     & / ( dlog(td(ndp)/td(i)) * dlog(td(ndp)/td(k)) )
     & - dlog(td(ndp)/td(k)) * pd(i)
     & / ( dlog(td(i)/td(k)) * dlog(td(ndp)/td(i)) )
c --
```

```
       a = 2* pd(k) / ( dlog(td(i)/td(k)) * dlog(td(ndp)/td(k)) )
     &   - 2* pd(i) / ( dlog(td(ndp)/td(i)) * dlog(td(i)/td(k)) )
     &   + 2*pd(ndp) / ( dlog(td(ndp)/td(k)) * dlog(td(ndp)/td(i)) )
c
c - computation of Laplace transform with linear interpolation between
c - data points, and power extrapolation afterwards
c
      f0 = (pd(1)-pinitl) / td(1)
      sum= f0 * (1. - dexp(-s*td(1)) ) / (s*s)
      do 1 i=1, ndp-1
         fi = (pd(i+1)-pd(i)) / (td(i+1)-td(i))
         sum = sum + fi * ( dexp(-s*td(i)) - dexp(-s*td(i+1)) ) / (s*s)
 1    continue
c - a log-log extrapolation for the derivative for large t -----------
      alpha= a / m
      alpha1=alpha+1.d0
      xn= s*td(ndp)
      if ( (dabs(alpha).gt.(1.d-1)) .and. (xn.lt.50) ) goto 68
c -  if the derivative is flat enough, the exponential integral is OK
      sum= sum+ m * expin(xn) / s
      flapl8 = sum
      return
 68    sum= sum + m / (alpha*s* xn**alpha)
     &         * ( DGAMIC(alpha1,xn) - xn**alpha *dexp(-xn) )
       flapl8 = sum
       return
       end
```

5.2 Field Example

The algorithms had to be validated not only on simulated data, to which noise had been added, but also on a difficult field case. This third example, called Well A, is a drawdown test on a partially penetrated well, in a formation known to be mildly layered. A $\approx$ 1,000-ft rathole is present below the producing zones. The well was put on production with the expectation that the production rate would stabilize at a constant rate of 15,000 B/D. Within a 20-minute period, a significant drop in the downhole pressure was noticed, and the production had to be decreased to avoid two-phase flow in the wellbore and formation (see flowrate in Fig. 5.1), resulting in a decreasing pressure drop after $\approx$ 30 min. Additionnally, data acquisition was halted after 7 hours of recording because of operational problems. This test is not interpretable without taking into account the flowrate history, and model recognition cannot be performed without deconvolution. The following for-

mula was used:

$$s_f \ \overline{\Delta p_{wc}}(s_f) \ = \ \frac{s_f \ \overline{\Delta p_w}(s_f)}{s_f \ \overline{q_m}(s_f)} \tag{5.1}$$

Regression (storage and skin match) was still performed in real space. Fig. 5.2 shows the result of deconvolution both in Laplace space and in real space. The hemispherical flow due to partial penetration is visible, as well as the slight double porosity behavior due to the layers. The results can be compared with those in Ref. [8]. The flapl8 algorithm was used to take the (forward) Laplace transform of both the pressure and flowrate data, and Stehfest algorithm was used (with n=4) to take the inverse Laplace transform. The results are good enough to make the Laplace approach interesting in practice for deconvolution problems.

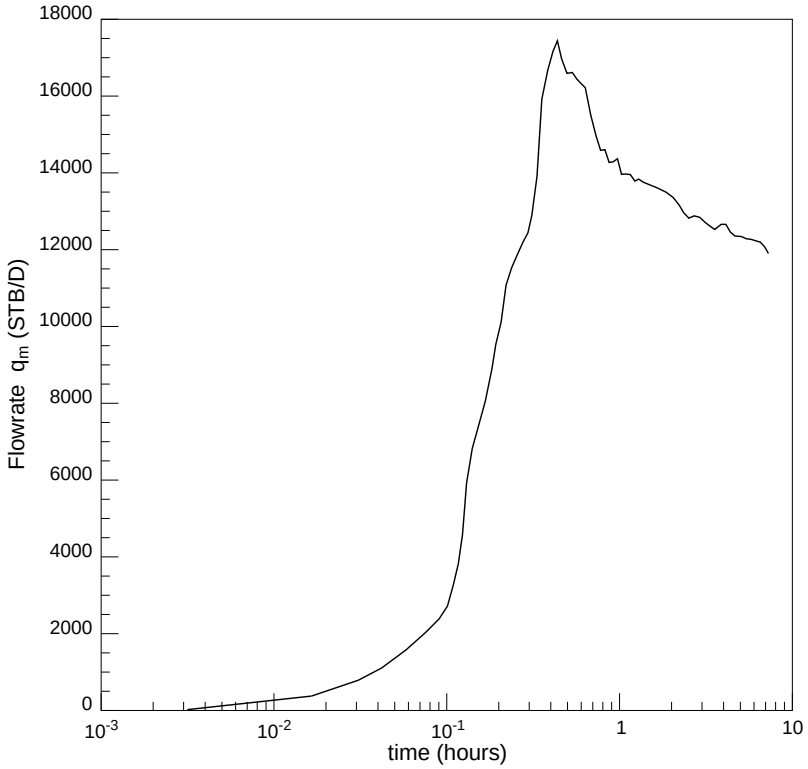

Figure 5.1: Well A: measured downhole flowrate (field data)

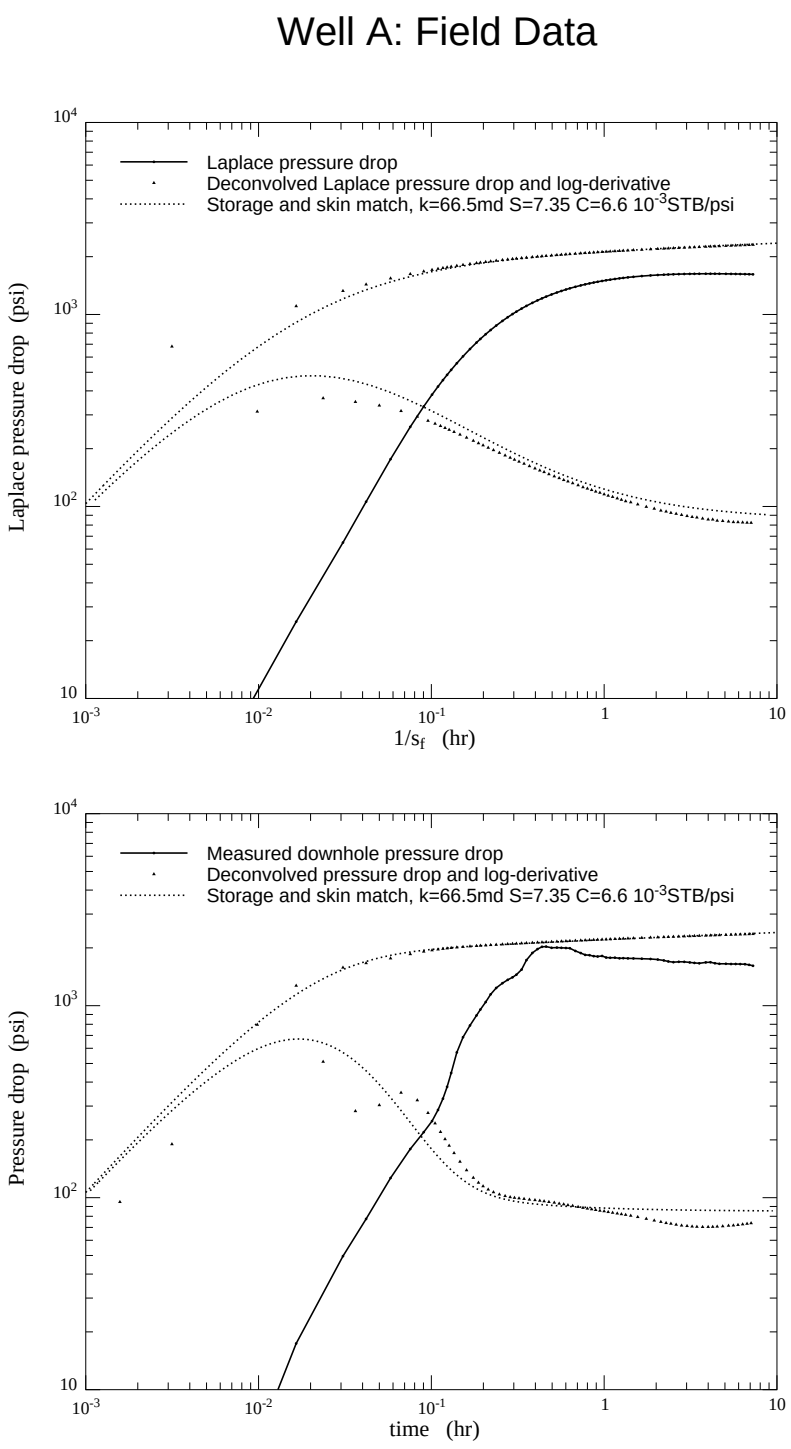

Figure 5.2: Well A: Deconvolved pressure drop in Laplace and real space